FAULT TOLERANT CONTROL OF HOMOPOLAR MAGNETIC BEARINGS AND CIRCULAR SENSOR ARRAYS

A Dissertation

by

MING-HSIU LI

Submitted to the Office of Graduate Studies of
Texas A&M University
in partial fulfillment of the requirements for the degree of

DOCTOR OF PHILOSOPHY

December 2004

Major Subject: Mechanical Engineering

FAULT TOLERANT CONTROL OF HOMOPOLAR MAGNETIC BEARINGS AND CIRCULAR SENSOR ARRAYS

A Dissertation

by

MING-HSIU LI

Submitted to Texas A&M University
in partial fulfillment of the requirements
for the degree of

DOCTOR OF PHILOSOPHY

Approved as to style and content by:

Alan B. Palazzolo (Chair of Committee)	Shankar P. Bhattacharyya (Member)
Alexander Parlos (Member)	Won-Jong Kim (Member)

Dennis O'Neal
(Head of Department)

December 2004

Major Subject: Mechanical Engineering

ABSTRACT

Fault Tolerant Control of Homopolar Magnetic Bearings and Circular Sensor Arrays.

(December 2004)

Ming-Hsiu Li, B.S., National Chung Hsing University; M.S., National Cheng Kung University, Taiwan

Chair of Advisory Committee: Dr. Alan B. Palazzolo

Fault tolerant control can accommodate the component faults in a control system such as sensors, actuators, plants, etc. This dissertation presents two fault tolerant control schemes to accommodate the failures of power amplifiers and sensors in a magnetic suspension system. The homopolar magnetic bearings are biased by permanent magnets to reduce the energy consumption. One control scheme is to adjust system parameters by swapping current distribution matrices for magnetic bearings and weighting gain matrices for sensor arrays, but maintain the MIMO-based control law invariant before and after the faults. Current distribution matrices are evaluated based on the set of poles (power amplifier plus coil) that have failed and the requirements for uncoupled force/voltage control, linearity, and specified force/voltage gains to be unaffected by the failure. Weighting gain matrices are evaluated based on the set of sensors that have failed and the requirements for uncoupling x_1 and x_2 sensing, runout reduction, and voltage/displacement gains to be unaffected by the failure. The other control scheme is to adjust the feedback gains on-line or off-line, but the current distribution matrices are

invariant before and after the faults. Simulation results have demonstrated the fault tolerant operation by these two control schemes.

DEDICATION

To my parents.

ACKNOWLEDGMENTS

First of all, I would like to thank Dr. Palazzolo for his patience to teach me, his guidance on this research, and the opportunity to work in the Vibration Control Electromagnetics Lab. I would also like to thank Dr. Shankar P. Bhattacharyya, Dr. Alexander Parlos, and Dr. Won-Jong Kim for serving on my advisory committee.

In addition, I would like to thank my colleagues, Dr. Shulinag Lei, Dr. Andrew Kenny, Dr. Yeonkyu Kim, and Dr. Guangyong Sun, for their valuable opinions and discussion. I also express my gratitude to NASA Glenn and the NASA Center for Space Power at Texas A&M for funding this work.

TABLE OF CONTENTS

CHAPTER Page

LIST OF FIGURES

FIGURE Page

FIGURE Page

LIST OF TABLES

CHAPTER I

INTRODUCTION

1.1 Overview

Fault tolerant control (FTC) can accommodate the component faults in a control system such as sensors, actuators, plants, etc. and in the meantime can maintain the acceptable performance. One of the objectives of FTC is to improve system reliability, especially for some systems where maintenance is not easy or convenient to do, like space stations, and which require higher safety concerns, like nuclear power plants and aircrafts. The normal redundant design is to add some backup components in the system. When the normal components fail, the redundant components can continue the operation.

A flywheel-based magnetic suspension system has the potential application as an energy storage system for space stations. Normally the flywheel is suspended by two magnetic bearings, which have many advantages over the traditional bearings such as no contact between the shaft and stator, no lubrication, high spin speed operation, and adjustable equivalent damping and stiffness, which are functions of controller parameters.

This dissertation follows the style and format of Journal of Dynamic Systems, Measurement, and Control.

To the use linear control technique, the linear relation between magnetic forces and currents can be preserved by the generalized bias linearization method. The bias flux can be supplied either by electric coils or by permanent magnets (PM). To reduce power consumption, the magnetic bearings biased by PMs can improve efficiency.

Sensor runout is a major disturbance in rotating machinery supported on magnetic bearing systems. Sensor runout results from geometrical, electrical, magnetic, or optical non-uniformity around the circumference of the shaft at the position sensor locations. Runout produces a false indication of the shaft centerlines position, thus generating unnecessary control currents and heating and pushing power amplifiers into slew rate saturation.

This dissertation is focused on the fault tolerant control of a flywheel-based magnetic suspension system that is suspended by two homopolar magnetic bearings (HOMB). These magnetic bearings are biased by permanent magnets to reduce the energy consumption and have redundant design, i.e., extra power amplifiers (PA) in a magnetic bearing. In addition, the similar fault tolerant control concept of the magnetic bearings is extended to the sensor system, which is called circular sensor arrays. The array has redundant design, i.e. extra sensors in an array. The objectives of the array are to eliminate the sensor runout and in the meantime improve the sensor system reliability.

Generally speaking, two control schemes are utilized to compensate for the power amplifier failures in magnetic bearings and the sensor failures in arrays. One is to swap the current distribution matrices (CDM) for the power amplifier failures and weighting gain matrices (WGM) for the sensor failures according to different failure

configurations. Under this approach, the MIMO-based PD (PID) control gains are invariant before and after the component faults. The other approach is to maintain the CDMs for the unfailed state invariant before and after the power amplifier failures. The MIMO-based feedback gains are updated off-line or on-line to compensate for the faults.

From the simulation results, the reliability of magnetic bearings and sensor arrays can be improved by fault tolerant control.

1.2 Literature Review

Attractive magnetic bearing actuators possess individual pole forces that vary quadratically with current. The net force of the bearing may be linearized with respect to the control voltages by utilizing a bias flux component [1,2]. Thus the X_1, X_2, and X_3 forces become decoupled, i.e., dependent only on their respective control voltages (V_{c1}, V_{c2}, and V_{c3}). Maslen and Meeker [3] provided a generalization of this approach for heteropolar magnetic bearings (HEMB), which derive their bias flux from electric coils and utilize both N and S at different poles.

FTC of HEMBs has been demonstrated on a 5 axis, flexible rotor test rig with 3 CPU failures and 2 (out of 8) adjacent coil failures [4]. CDMs for HEMBs were extended to cover 5 pole failures out of 8 poles [5,6] and for the case of significant effects of material path reluctance and fringing [7].

The fault tolerant approach outlined above utilizes a CDM that changes the current in each pole after failure in order to achieve linearized, decoupled relations between control forces and control voltages. A failure configuration is defined by the

subset of poles that fail due either to shorting of a turn in a coil or to failure of a power amplifier. In general there exist (2^n-1) number of possible failure configurations for an n pole magnetic bearing. The concept of CDM is extended to the HOMBs in this dissertation. The HOMBs commonly use permanent magnets for its bias flux to increase the actuator's efficiency and reduce heat generation [8]. Points on the surface of the spinning journal in the homopolar bearing do not experience north-south flux reversals, thereby reducing rotor losses due to hysteresis and eddy currents.

There are two approaches for runout rejection in the controller stages. The first is use of notch filters inserted in the control loop at harmonics of the spin frequency [9]. The main drawback to this is that the phase lag caused by the notch filter may destabilize the closed loop system [10,11]. To preserve the stability, Herzog et al. [12] proposed a generalized narrow-band notch filter which is inserted into the multivariable feedback without destabilizing the closed loop. The other approach is to use adaptive feedforward compensation of unbalance. Na and Park [13] developed an adaptive feedforward controller for the rejection of periodic disturbances without changing closed loop characteristics. Knospe et al. [14-17] presented an adaptive gain matrix to suppress the unbalance vibration of rotors supported in magnetic bearings, and steady state performance is robust to structure uncertainty. For sensor runout, Kim and Lee [18] used the extended influence coefficient method [16] to identify and eliminate runout. Setiawan et al. [19,20] presented an adaptive algorithm for sensor runout compensation that is robust to plant parameter uncertainties.

The cited references concentrate on the spin frequency component of runout. Experience indicates that higher harmonics may also cause saturation of the power amplifier and excess heating. This dissertation presents a circular array of sensors and WGMs for reducing multiple harmonics of runout even with failed sensors.

Adaptive control systems can accommodate the uncertainties of the plant, components (sensor and actuator), and environment (disturbance). Tao et al. [21-23] developed the adaptive control schemes to compensate for a class of actuator failures where some of the plant inputs are stuck at fixed values.

Without swapping the CDMs according to different failure combinations of the power amplifiers, it will make some system parameters (control voltage stiffness) jump. Two adaptive control schemes are utilized to accommodate the jump parameters. The gain scheduling adaptive control scheme is combined with the signal-based fault detection. The adaptive pole placement control (APPC) scheme is combined with the model-based fault detection (estimator).

1.3 Objectives

In this dissertation, two control schemes are utilized to implement the FTC of a flywheel-based magnetic suspension that can accommodate the failures of power amplifiers and sensors. One is to adjust the system parameters: the entries of CDMs for the magnetic bearings and the entries of WGMs for the sensor arrays. Thus, the MIMO-based PD (PID) control law is invariant before and after the faults. The other control

scheme is to adjust the MIMO-based feedback gains off-line or on-line, but maintain the same CDMs for the unfailed state.

1.4 Organization

Chapter II presents the FTC of HOMBs, including the CDMs of homopolar combo bearings (HCB) and homopolar radial bearings (HRB), de-coupling chokes, the dynamic model of a flywheel-based magnetic suspension, the MIMO-based PD (PID) control law, the reliability of a magnetic bearing, and simulations with power amplifier failures.

Chapter III presents the FTC of sensor arrays, including the WGM, sensor array reliability, runout reduction probability, and simulation with sensor failures. The MIMO-based PD (PID) control law in Chapters II and III are invariant before and after the faults.

Chapter IV utilizes the adaptive control to compensate for the failures of power amplifiers. The CDMs for the unfailed state are invariant before and after the faults. This includes a simplified dynamic model of a magnetic suspension system, gain scheduling adaptive control scheme, adaptive pole placement control scheme, and simulations with power amplifier failures by adaptive control.

Chapter V summarizes some interesting trends of FTC. The future of this research direction is also discussed in this chapter.

CHAPTER II

FAULT-TOLERANT HOMOPOLAR MAGNETIC BEARINGS*

Magnetic suspensions satisfy the long life and low loss conditions demanded by satellite and International Space Station (ISS) based flywheels used for Attitude Control and Energy Storage (ACES) service. This chapter summarizes the development of a novel magnetic suspension that improves reliability via fault tolerant control (FTC). Specifically, flux coupling between poles of a homopolar magnetic bearing (HOMB) is shown to deliver desired forces even after termination of coil currents to a subset of "failed poles." Linear, coordinate decoupled force–voltage relations are also maintained before and after failure by bias linearization. Current distribution matrices (CDM) which adjust the currents and fluxes following a pole set failure are determined for many faulted pole combinations. The CDMs for the homopolar combo bearing (HCB) are (n+2)-by-3 matrices, and the CDMs for the homopolar radial bearing (HRB) are n-by-2 matrices, where n is the number of radial poles. The CDMs and the system responses are obtained utilizing 1D magnetic circuit models with fringe and leakage factors derived from detailed, 3D, finite element field models. Reliability is based on the success criterion that catcher bearing-shaft contact does not occur following pole failures. The magnetic bearing reliability is improved by increasing the number of the radial poles.

2.1 Current Distribution Matrix of Homopolar Magnetic Bearings

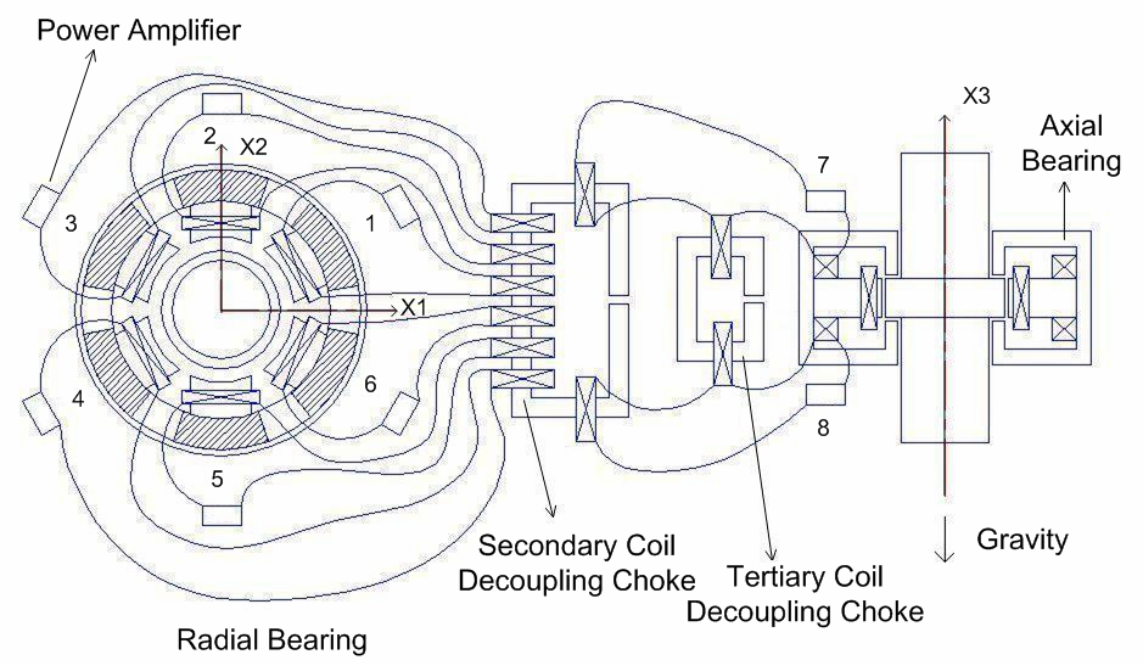

Fig. 2.1 Six Pole Homopolar Combo Bearing.

Derivation of the FTC approach requires applications of Ampere's, Ohm's, Faraday's Laws and the Maxwell Stress Tensor to the multi-path magnetic circuit in a magnetic bearing. The physical requirements of CDM include

(a) De-coupling Condition: The x_i control voltage does not affect the x_j control force unless i = j, where the triple $(x_1 \quad x_2 \quad x_3)$ is the Cartesian coordinate.

(b) Linearity Condition: The x_i control voltage and x_i control force are linearly related.

(c) Invariance Condition 1: The force/voltage gains are not affected by the failure.

(d) Invariance Condition 2: The force/position gains are not affected by the failure.

The FTC requirement (d) is automatically satisfied for a magnetic bearing with bias fluxes generated by permanent magnets located circumferentially and in equal space. This results since the permanent and the resulting bias flux are unaffected by the failure state of the poles.

A complete derivation of the FTC theory is developed next for a 6 pole homopolar combination (combo, radial and axial forces) magnetic bearing. The FTC theory for the 4 and 7 pole bearings is very similar and is not included.

Figure 2.1 depicts a combination (radial/axial) 6 pole HCB installed on a vertically directed shaft. The actuator has 6 radial poles and coils and 2 axial poles and coils. The axial coils are wound circumferentially around the shaft, and the radial coils are wound around the poles. The coil leads also form secondary coils around a common de-coupling choke, and the axial leads also form tertiary coils around a second de-coupling choke. The de-coupling chokes eliminate mutual inductances and insure that the inductance matrix is non-singular, which insures electric circuit stability [2]. The laminated construction provides for an accurate approximation of infinite bandwidth between currents and fluxes. Following common practice, the actuator is modeled as an equivalent magnetic circuit with de-rated magnetic strength accounting for leakage and de-rated gap flux density to account for fringing. Figure 2.2 shows the 6 flux paths through the radial poles and 2 flux paths through the axial poles.

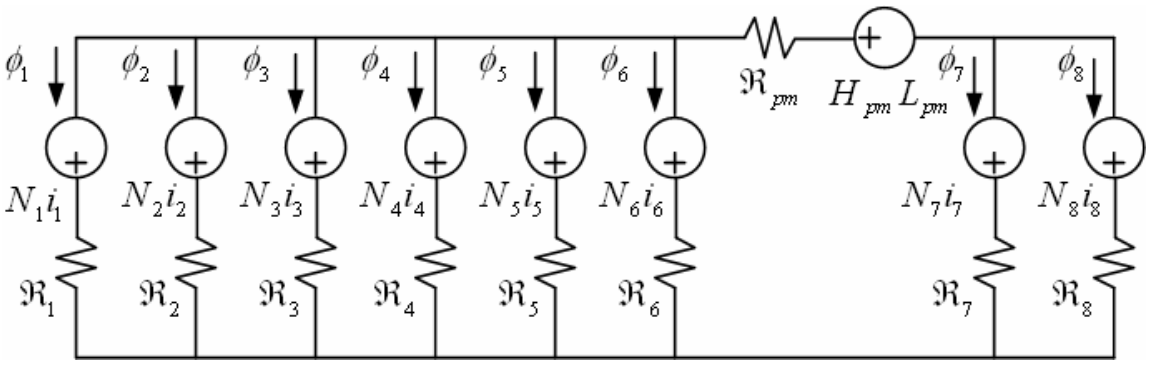

Fig. 2.2 Equivalent Magnetic Circuit for the Six Pole Homopolar Combo Bearing.

The magnetic circuit provides a useful tool to present flux conservation and Ampere Law relations with an equivalent electric circuit model. Kirchhoff's law applied to Fig. 2.2 yields

$$\begin{bmatrix} \Re_1 & -\Re_2 & 0 & 0 & 0 & 0 & 0 & 0 \\ 0 & \Re_2 & -\Re_3 & 0 & 0 & 0 & 0 & 0 \\ 0 & 0 & \Re_3 & -\Re_4 & 0 & 0 & 0 & 0 \\ 0 & 0 & 0 & \Re_4 & -\Re_5 & 0 & 0 & 0 \\ 0 & 0 & 0 & 0 & \Re_5 & -\Re_6 & 0 & 0 \\ \Re_{pm} & \Re_{pm} & \Re_{pm} & \Re_{pm} & \Re_{pm} & \Re_{pm}+\Re_6 & -\Re_7 & 0 \\ 0 & 0 & 0 & 0 & 0 & 0 & \Re_7 & -\Re_8 \\ 1 & 1 & 1 & 1 & 1 & 1 & 1 & 1 \end{bmatrix} \begin{bmatrix} \phi_1 \\ \phi_2 \\ \phi_3 \\ \phi_4 \\ \phi_5 \\ \phi_6 \\ \phi_7 \\ \phi_8 \end{bmatrix} =$$

$$\begin{bmatrix} N_1 & -N_2 & 0 & 0 & 0 & 0 & 0 & 0 \\ 0 & N_2 & -N_3 & 0 & 0 & 0 & 0 & 0 \\ 0 & 0 & N_3 & -N_4 & 0 & 0 & 0 & 0 \\ 0 & 0 & 0 & N_4 & -N_5 & 0 & 0 & 0 \\ 0 & 0 & 0 & 0 & N_5 & -N_6 & 0 & 0 \\ 0 & 0 & 0 & 0 & 0 & N_6 & -N_7 & 0 \\ 0 & 0 & 0 & 0 & 0 & 0 & N_7 & -N_8 \\ 0 & 0 & 0 & 0 & 0 & 0 & 0 & 0 \end{bmatrix} \begin{bmatrix} i_1 \\ i_2 \\ i_3 \\ i_4 \\ i_5 \\ i_6 \\ i_7 \\ i_8 \end{bmatrix} + \begin{bmatrix} 0 \\ 0 \\ 0 \\ 0 \\ 0 \\ H_{pm}L_{pm} \\ 0 \\ 0 \end{bmatrix}$$

$$R\Phi = NI + H \tag{2.1}$$

where

$$\Re_i = g_i /(\mu_0 a_i) \tag{2.2}$$

In (2.1) the symbols $\Re_{(\ )}$, $\phi_{(\ )}$, $N_{(\ )}$, $i_{(\ )}$, H_{pm}, and L_{pm} are the reluctance, flux, number of turns of a coil, current, and the coercive force and length of a permanent magnet, respectively. In (2.2) the symbols $g_{(\ )}$, $a_{(\ )}$, and μ_0 are the pole gap and face area and permeability of free space. Let A represent a diagonal matrix of pole gap areas then by assuming uniform flux densities in each gap

$$AB = \Phi \tag{2.3}$$

where B is the flux density vector. Substituting (2.3) into (2.1) yields

$$B = VI + B_{bias} \tag{2.4}$$

where

$$V = A^{-1}R^{-1}N \tag{2.5}$$

$$B_{bias} = A^{-1}R^{-1}H \tag{2.6}$$

Equation (2.4) shows that the control flux varies with control current and with shaft position (gap values), however the bias flux varies solely with shaft position.

Magnetic bearings typically utilize servo power amplifiers that provide 1.2-2.0 kHz bandwidth for inductive loads ranging between 2 mH and 8 mH. Thus it is acceptable to use a constant for the control current per control voltage gain. Let

$$V_c = (V_{c1} \quad V_{c2} \quad V_{c3})^T \tag{2.7}$$

represent the control voltages and the matrix T is the CDM. Then in the absence of pole failures

$$I' = TV_c \tag{2.8}$$

where T includes the power amplifier gain and the current distribution terms. Fault conditions are represented using the matrix K that has a null row for each faulted pole. Then the failed actuator control currents become

$$I = KI' = KTV_c \tag{2.9}$$

For example if coils 1 and 2 fail

$$K = diag\begin{pmatrix}0 & 0 & 1 & 1 & 1 & 1 & 1 & 1\end{pmatrix} \tag{2.10}$$

The magnetic forces are determined from the Maxwell stress tensor as

$$F_j = B^T \gamma_j B \qquad j = 1,2,3 \tag{2.11}$$

where γ_j are 8-by-8 matrices and given as

$$\gamma_1 = diag[a_i \cos\theta_i /(2\mu_0)], i = 1 \sim 6,\ \gamma_1(7,7) = \gamma_1(8,8) = 0 \tag{2.12}$$

$$\gamma_2 = diag[a_i \sin\theta_i /(2\mu_0)], i = 1 \sim 6,\ \gamma_2(7,7) = \gamma_2(8,8) = 0 \tag{2.13}$$

$$\gamma_3(7,7) = -\gamma_3(8,8) = a^{'} /(2\mu_0)\text{, all other components are zero} \tag{2.14}$$

where θ_i is the angle between the ith pole and axis x_1 and a' is the face area of the axial poles. Substituting (2.9) into (2.4) yields

$$B = WV_c + B_{bias} \tag{2.15}$$

where $W = VKT$. The magnetic forces are given in terms of control voltages and bias flux density as

$$F_j = V_c{}^T W^T \gamma_j W V_c + 2B_{bias}^T \gamma_j W V_c + B_{bias}^T \gamma_j B_{bias} \qquad j = 1,2,3 \tag{2.16}$$

The magnetic forces are proportional to the square of control voltages in (2.16). The following constraint equations must be satisfied in order to meet FTC requirements (a), (b), and (c).

$$W^T \gamma_1 W = 0_{3\times 3} \tag{2.17}$$

$$2B_{bias}^T \gamma_1 W = \begin{bmatrix} k_{v1} & 0 & 0 \end{bmatrix} \tag{2.18}$$

$$W^T \gamma_2 W = 0_{3\times 3} \tag{2.19}$$

$$2B_{bias}^T \gamma_2 W = \begin{bmatrix} 0 & k_{v2} & 0 \end{bmatrix} \tag{2.20}$$

$$W^T \gamma_3 W = 0_{3\times 3} \tag{2.21}$$

$$2B_{bias}^T \gamma_3 W = \begin{bmatrix} 0 & 0 & k_{v3} \end{bmatrix} \tag{2.22}$$

where the scalars k_{v1}, k_{v2}, k_{v3} are desired control voltage stiffness. Equations (2.17) to (2.22) are 18 nonlinear and 9 linear algebraic equations for the CDM entries, t_{ij}. The CDM entries are obtained by requiring simultaneous solution of these constraint equations and minimization of the Frobenius matrix norm of the CDM. This is typically performed at the magnetic center, i.e. the location where the bias flux balances the static loads on the bearing. The norm of the current vector, I in (2.9), satisfies the consistency condition [24]

$$\|I\| \le \|K\| \cdot \|T\| \cdot \|V_c\| \tag{2.23}$$

where for a Frobenius norm

$$\|K\| = \sqrt{\sum_{i,j} K_{ij}^{\ 2}} \tag{2.24}$$

$$\|T\| = \sqrt{\sum_{i,j} t_{ij}^{\,2}} \tag{2.25}$$

$$\|V_c\| = \sqrt{\sum_{i} V_{ci}^{\,2}} \tag{2.26}$$

Thus by (2.23) reduction of $\|I\|$ follows from minimizing $\|T\|$. The Lagrange multiplier approach is employed to locate a solution of the equations in (2.17) to (2.22), that minimize $\|T\|$. The cost function is

$$L = \sum_{i=1}^{p}\sum_{j=1}^{3} t_{ij}^{\,2} + \sum_{k=1}^{27} \lambda_k h_k \tag{2.27}$$

where p is the number of functioning poles, λ_k are the Lagrange multipliers and h_k are the 27 constraint equations. The solution condition is

$$\frac{\partial L}{\partial Z_m} = 0 \ , \quad Z_m \in \{t_{ij}, \lambda_k\} \tag{2.28}$$

which implies

$$F(t_{ij}, \lambda_k) = \left[h_1 \ \cdots \ h_{27} \ \ \frac{\partial L}{\partial t_{11}} \ \ \frac{\partial L}{\partial t_{12}} \ \ \frac{\partial L}{\partial t_{13}} \ \cdots \ \frac{\partial L}{\partial t_{p1}} \ \ \frac{\partial L}{\partial t_{p2}} \ \ \frac{\partial L}{\partial t_{p3}} \right]^T = 0 \tag{2.29}$$

For the 6 pole HCB the total set of equations is over-determined, i.e. more equations than unknowns (at most 24 unknowns), therefore a solution exists only in the least square sense. The nonlinear equation, least square based solver available in MATLAB is employed for this purpose. The effectiveness of each solution in satisfying the FTC requirements must be checked by transient response simulation of the respective fault event since the least square solution is not exact.

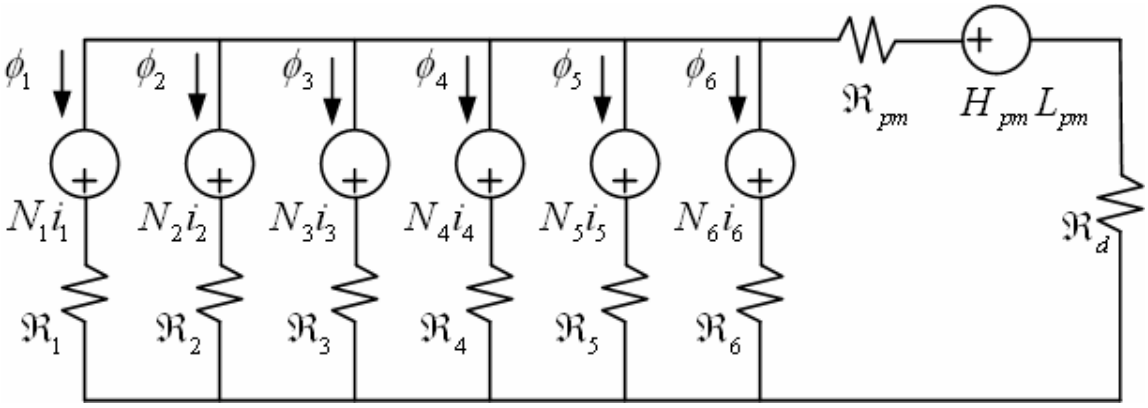

Fig. 2.3 Equivalent Magnetic Circuit for the Six Pole Homopolar Radial Bearing.

The 6 pole HRB provides force solely in the two transverse (radial) directions. A magnetic circuit model for this bearing is illustrated in Fig. 2.3. The flux-current relations for this circuit are obtained by applying Kirchoff's laws, which yield

$$\begin{bmatrix} \Re_1 & -\Re_2 & 0 & 0 & 0 & 0 \\ 0 & \Re_2 & -\Re_3 & 0 & 0 & 0 \\ 0 & 0 & \Re_3 & -\Re_4 & 0 & 0 \\ 0 & 0 & 0 & \Re_4 & -\Re_5 & 0 \\ 0 & 0 & 0 & 0 & \Re_5 & -\Re_6 \\ \Re_d + \Re_{pm} & \Re_d + \Re_{pm} & \Re_d + \Re_{pm} & \Re_d + \Re_{pm} & \Re_d + \Re_{pm} & \Re_d + \Re_{pm} + \Re_6 \end{bmatrix} \begin{bmatrix} \phi_1 \\ \phi_2 \\ \phi_3 \\ \phi_4 \\ \phi_5 \\ \phi_6 \end{bmatrix} =$$

$$\begin{bmatrix} N_1 & -N_2 & 0 & 0 & 0 & 0 \\ 0 & N_2 & -N_3 & 0 & 0 & 0 \\ 0 & 0 & N_3 & -N_4 & 0 & 0 \\ 0 & 0 & 0 & N_4 & -N_5 & 0 \\ 0 & 0 & 0 & 0 & N_5 & -N_6 \\ 0 & 0 & 0 & 0 & 0 & N_6 \end{bmatrix} \begin{bmatrix} i_1 \\ i_2 \\ i_3 \\ i_4 \\ i_5 \\ i_6 \end{bmatrix} + \begin{bmatrix} 0 \\ 0 \\ 0 \\ 0 \\ 0 \\ H_{pm} L_{pm} \end{bmatrix} \tag{2.30}$$

where

$$\Re_d = \sqrt{g_{0d}^2 - x_1^2 - x_2^2} / (\mu_0 a_d) \tag{2.31}$$

In (2.31) symbols g_{0d} and a_d are the air gap and face area of the dead pole of the HRB. The FTC requirements result in 10 constraint equations

$$W^T \gamma_1 W = 0_{2\times 2} \tag{2.32}$$

$$2B_{bias}^T \gamma_1 W = \begin{bmatrix} k_{v1} & 0 \end{bmatrix} \tag{2.33}$$

$$W^T \gamma_2 W = 0_{2\times 2} \tag{2.34}$$

$$2B_{bias}^T \gamma_2 W = \begin{bmatrix} 0 & k_{v2} \end{bmatrix} \tag{2.35}$$

where γ_1 and γ_2 are 6-by-6 matrices, which are similar to (2.12) and (2.13). These equations are solved for t_{ij} and λ_k utilizing the Lagrange multiplier / nonlinear least square solver approach discussed for the 6 pole HCB.

2.2 De-coupling Choke

The inductance matrix of the isolated combo bearing is singular because flux conservation introduces a dependency relation between the fluxes. This produces a potentially unstable operation state for the power amplifiers. Two de-coupling chokes are added to the combo bearing according to Meeker's approach [2]. By adjusting the parameters of the de-coupling chokes (N_{c1}, N_{c2}, N_{c3}, $\Re_{c1}$, $\Re_{c2}$) the inductance matrix becomes full rank and the mutual inductances become zero. Similarly, a single de-coupling choke is added to the radial bearing.

2.3 Dynamic Model of a Magnetic Suspension System

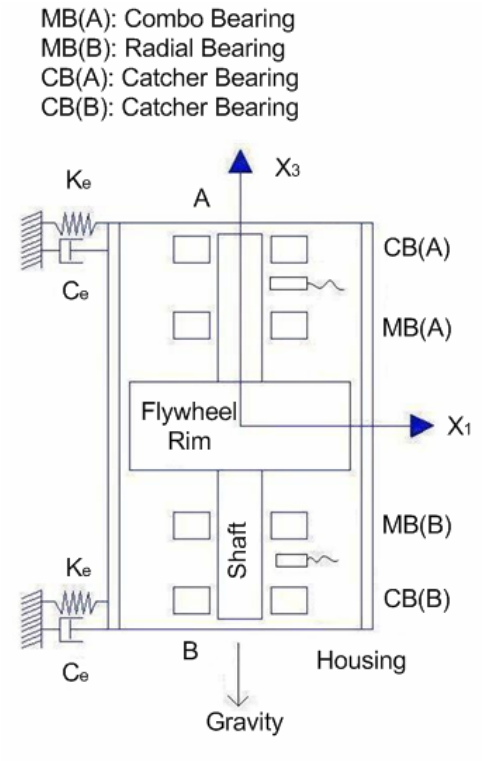

Fig. 2.4 Flywheel System with a Magnetic Suspension.

The novel redundant actuators operate within a feedback controlled system that includes both electrical component and structural component dynamics. A typical application is a flywheel module consisting of a high speed shaft, integrally mounted motor-generator, composite flywheel rim, magnetic suspension, and flexibly mounted housing. Figure 2.4 depicts a module model with 9 rigid body structural degrees of freedom: rotor CG translations (x_{1r}, x_{2r}, x_{3r}), rotor rotations $(\theta_{1r}, \theta_{2r})$, housing CG translations (x_{1h}, x_{2h}), and housing rotation $(\theta_{1h}, \theta_{2h})$. The magnetic suspension

employs magnetic (MB) and backup (catcher, CB) bearings at both the A and B ends of the module. Magnetic bearing clearances are approximately 0.5 mm so small angle motion may be assumed. The equations of motion then become

$$\begin{bmatrix} m_r & 0 & 0 & 0 & 0 \\ 0 & I_{tr} & 0 & 0 & 0 \\ 0 & 0 & m_r & 0 & 0 \\ 0 & 0 & 0 & I_{tr} & 0 \\ 0 & 0 & 0 & 0 & m_r \end{bmatrix} \begin{bmatrix} \ddot{x}_{1r} \\ \ddot{\theta}_{1r} \\ \ddot{x}_{2r} \\ \ddot{\theta}_{2r} \\ \ddot{x}_{3r} \end{bmatrix} + \begin{bmatrix} 0 & 0 & 0 & 0 & 0 \\ 0 & 0 & 0 & I_{pr}\omega & 0 \\ 0 & 0 & 0 & 0 & 0 \\ 0 & -I_{pr}\omega & 0 & 0 & 0 \\ 0 & 0 & 0 & 0 & 0 \end{bmatrix} \begin{bmatrix} \dot{x}_{1r} \\ \dot{\theta}_{1r} \\ \dot{x}_{2r} \\ \dot{\theta}_{2r} \\ \dot{x}_{3r} \end{bmatrix} = \begin{bmatrix} 1 & 0 & 0 & 1 & 0 \\ 0 & -L_{br}^A & 0 & 0 & L_{br}^B \\ 0 & 1 & 0 & 0 & 1 \\ L_{br}^A & 0 & 0 & -L_{br}^B & 0 \\ 0 & 0 & 1 & 0 & 0 \end{bmatrix} \begin{bmatrix} F_{1b}^A \\ F_{2b}^A \\ F_{3b}^A \\ F_{1b}^B \\ F_{2b}^B \end{bmatrix} +$$
$$\begin{bmatrix} 1 & 0 & 0 & 1 & 0 \\ 0 & -L_{cr}^A & 0 & 0 & L_{cr}^B \\ 0 & 1 & 0 & 0 & 1 \\ L_{cr}^A & 0 & 0 & -L_{cr}^B & 0 \\ 0 & 0 & 1 & 0 & 0 \end{bmatrix} \begin{bmatrix} F_{1c}^A \\ F_{2c}^A \\ F_{3c}^A \\ F_{1c}^B \\ F_{2c}^B \end{bmatrix} + \begin{bmatrix} 1 & 0 & 1 & 0 \\ 0 & -L_{dr}^A & 0 & L_{dr}^B \\ 0 & 1 & 0 & 1 \\ L_{dr}^A & 0 & -L_{dr}^B & 0 \\ 0 & 0 & 0 & 0 \end{bmatrix} \begin{bmatrix} F_{1d}^A \\ F_{2d}^A \\ F_{1d}^B \\ F_{2d}^B \end{bmatrix} + \begin{bmatrix} 0 \\ 0 \\ 0 \\ 0 \\ -m_r g \end{bmatrix}$$

$$M_r \ddot{X}_r + G_r \dot{X}_r = \left(T_r^{MB}\right)^T \hat{F}_{br} + \left(T_r^{CB}\right)^T \hat{F}_{cr} + B_{dr}\hat{F}_{dr} + F_{gr} \tag{2.36}$$

$$\begin{bmatrix} m_h & 0 & 0 & 0 \\ 0 & I_{t1h} & 0 & 0 \\ 0 & 0 & m_h & 0 \\ 0 & 0 & 0 & I_{t2h} \end{bmatrix} \begin{bmatrix} \ddot{x}_{1h} \\ \ddot{\theta}_{1h} \\ \ddot{x}_{2h} \\ \ddot{\theta}_{2h} \end{bmatrix} + \begin{bmatrix} 2 & 0 & 0 & L_{eh}^A - L_{eh}^B \\ 0 & (L_{eh}^A)^2 + (L_{eh}^B)^2 & -L_{eh}^A + L_{eh}^B & 0 \\ 0 & -L_{eh}^A + L_{eh}^B & 2 & 0 \\ L_{eh}^A + L_{eh}^B & 0 & 0 & (L_{eh}^A)^2 + (L_{eh}^B)^2 \end{bmatrix} \left(C_e \begin{bmatrix} \dot{x}_{1h} \\ \dot{\theta}_{1h} \\ \dot{x}_{2h} \\ \dot{\theta}_{2h} \end{bmatrix} + K_e \begin{bmatrix} x_{1h} \\ \theta_{1h} \\ x_{2h} \\ \theta_{2h} \end{bmatrix} \right)$$
$$= -\begin{bmatrix} 1 & 0 & 1 & 0 \\ 0 & -L_{bh}^A & 0 & L_{bh}^B \\ 0 & 1 & 0 & 1 \\ L_{bh}^A & 0 & -L_{bh}^B & 0 \end{bmatrix} \begin{bmatrix} F_{1b}^A \\ F_{2b}^A \\ F_{1b}^B \\ F_{2b}^B \end{bmatrix} - \begin{bmatrix} 1 & 0 & 1 & 0 \\ 0 & -L_{ch}^A & 0 & L_{ch}^B \\ 0 & 1 & 0 & 1 \\ L_{ch}^A & 0 & -L_{ch}^B & 0 \end{bmatrix} \begin{bmatrix} F_{1c}^A \\ F_{2c}^A \\ F_{1c}^B \\ F_{2c}^B \end{bmatrix} + \begin{bmatrix} 0 \\ 0 \\ 0 \\ -m_h g \end{bmatrix}$$

$$\begin{aligned} M_h \ddot{X}_h + G_h (C_e \dot{X}_h + K_e X_h) &= -\left(T_h^{MB}\right)^T \hat{F}_{bh} - \left(T_h^{CB}\right)^T \hat{F}_{ch} + F_{gh} \\ &= -\left(T_h^{MB}\right)^T T_{rh} \hat{F}_{br} - \left(T_h^{CB}\right)^T T_{rh} \hat{F}_{cr} + F_{gh} \end{aligned} \tag{2.37}$$

where

$$T_{rh} = \begin{bmatrix} 1 & 0 & 0 & 0 & 0 \\ 0 & 1 & 0 & 0 & 0 \\ 0 & 0 & 0 & 1 & 0 \\ 0 & 0 & 0 & 0 & 1 \end{bmatrix} \tag{2.38}$$

The symbols m_r, I_{tr}, I_{pr}, and ω in (2.36) are the rotor mass, transverse and polar moments of inertia, and spin frequency. The symbols m_h, I_{t1h}, I_{t2h}, K_e, and C_e in (2.37) are the housing mass, transverse moments of inertia, and the stiffness and damping of the support system. The symbol $L_{(\ )}^{(\ )}$ denotes the distances measured from the rotor or housing centers of mass to components. The sub-script denotes the components, and the super-script denotes the component locations at end A or B.

The CG coordinates (X_r, X_h) and bearing coordinates $(\hat{X}_r, \hat{X}_h)$ satisfy the following transformations.

$$\hat{X}_r = T_r^{(\ )} X_r \tag{2.39}$$

$$\hat{X}_h = T_h^{(\ )} X_h \tag{2.40}$$

where

$$\hat{X}_r = \begin{bmatrix} x_{1r}^A & x_{2r}^A & x_{3r}^A & x_{1r}^B & x_{2r}^B \end{bmatrix}^T \tag{2.41}$$

$$\hat{X}_h = \begin{bmatrix} x_{1h}^A & x_{2h}^A & x_{1h}^B & x_{2h}^B \end{bmatrix}^T \tag{2.42}$$

The super-script in (2.39) and (2.40) denotes the components: MB for magnetic bearings, CB for catcher bearings, and SE for sensors.

The nonlinear magnetic forces $\begin{pmatrix} F_{1b}^A & F_{2b}^A & F_{3b}^A & F_{1b}^B & F_{2b}^B \end{pmatrix}$ are determined by (2.16), and the catcher bearing model shown in Fig. 2.5 is employed for calculating the reaction forces $\begin{pmatrix} F_{1c}^A & F_{2c}^A & F_{3c}^A & F_{1c}^B & F_{2c}^B \end{pmatrix}$ when the rotor and catcher bearings contact. The symbols K_c, C_c, and μ are the contact stiffness, damping, and dynamic friction

coefficient, respectively. More sophisticated models with internal dynamics of races and balls or rollers are available [25] and could also be used in the system dynamics model.

The mass imbalance disturbance in the model is described by

$$F_{1d}^{A} = m_r e\omega^2 \cos\omega t \tag{2.43}$$

$$F_{2d}^{A} = m_r e\omega^2 \sin\omega t \tag{2.44}$$

$$F_{1d}^{B} = m_r e\omega^2 \cos(\omega t + \psi) \tag{2.45}$$

$$F_{2d}^{B} = m_r e\omega^2 \sin(\omega t + \psi) \tag{2.46}$$

where e is the rotor eccentricity and ψ is the phase angle.

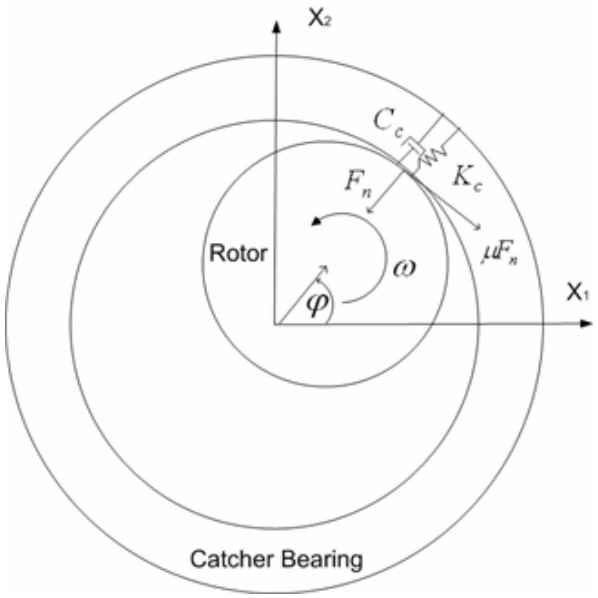

Fig. 2.5 Catcher Bearing Contact Model.

The EOMs in (2.36) and (2.37) can be expressed in terms of state space form.

$$\dot{X}_p = A_p X_p + B_{pb}\hat{F}_{br} + B_{pc}\hat{F}_{cr} + B_{pd}\hat{F}_{dr} + F_g \tag{2.47}$$

where

$$X_p = \begin{bmatrix} X_r^T & X_h^T & \dot{X}_r^T & \dot{X}_h^T \end{bmatrix}^T \tag{2.48}$$

$$A_p = \begin{bmatrix} 0_{5\times5} & 0_{5\times4} & I_{5\times5} & 0_{5\times4} \\ 0_{4\times5} & 0_{4\times4} & 0_{4\times5} & I_{4\times4} \\ 0_{5\times5} & 0_{5\times4} & -M_r^{-1}G_r & 0_{5\times4} \\ 0_{4\times5} & -M_h^{-1}G_hK_e & 0_{4\times5} & -M_h^{-1}G_hC_e \end{bmatrix} \tag{2.49}$$

$$B_{pb} = \begin{bmatrix} 0_{5\times5} \\ 0_{4\times5} \\ M_r^{-1}\left(T_r^{MB}\right)^T \\ -M_h^{-1}\left(T_h^{MB}\right)^T T_{rh} \end{bmatrix} \tag{2.50}$$

$$B_{pc} = \begin{bmatrix} 0_{5\times5} \\ 0_{4\times5} \\ M_r^{-1}\left(T_r^{CB}\right)^T \\ -M_h^{-1}\left(T_h^{CB}\right)^T T_{rh} \end{bmatrix} \tag{2.51}$$

$$B_{pd} = \begin{bmatrix} 0_{5\times4} \\ 0_{4\times4} \\ M_r^{-1}B_{dr} \\ 0_{4\times4} \end{bmatrix} \tag{2.52}$$

$$F_g = \begin{bmatrix} 0_{5\times1} \\ 0_{4\times1} \\ M_r^{-1}F_{gr} \\ M_h^{-1}F_{gh} \end{bmatrix} \tag{2.53}$$

2.4 MIMO-based PD (PID) Control Law

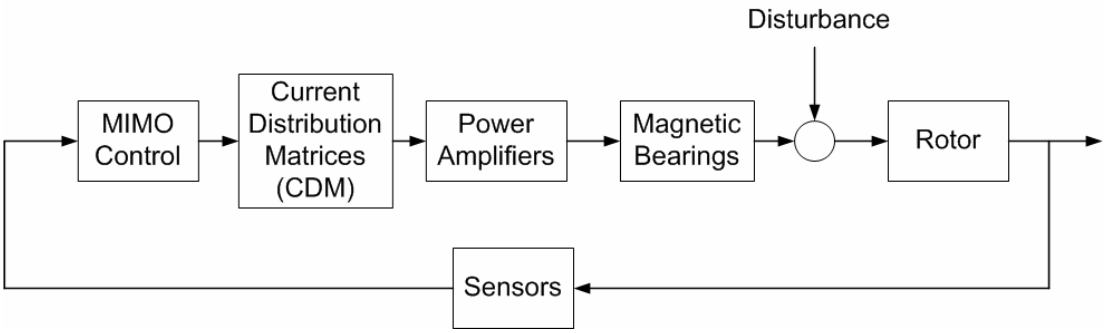

Fig. 2.6 Magnetic Suspension Control Scheme.

The control law utilized in the model is MIMO based and similar to the work of Okada [26] and Ahrens [27,28]. Figure 2.6 illustrates the overall feedback control loop for the magnetic suspension. Five PD (PID) controllers are coupled. (n+2) power amplifiers are utilized for the combo bearing and n power amplifiers for the radial bearing. Five displacement sensors measure the relative displacements between the rotor and housing. CDMs for the combo and radial bearings are incorporated in the controllers to produce reference voltages for the (2n+2) power amplifiers which produce the desired currents in each coil.

The current produced by a power amplifier is turned off at the moment of failure which simulates an open circuit. This is implemented in the model by changing the K matrix in (2.9) from the identity matrix to its pole-failed value, while the no-pole failed CDM is retained. The appropriate CDM for the pole-failure configuration being tested is

then swapped in following a delay time. The MIMO control law in Fig. 2.6 is invariant throughout the entire simulation.

2.5 Reliability of a Magnetic Bearing

The “k-out-of-n” system structure is a popular redundant design to improve the system reliability. The definition of “k-out-of-n: G” system structure in [29] is given as: An n-component system works if and only if at least k of the n components work. The redundant design for the magnetic bearings in Fig. 1 is similar to the “k-out-of-n” system structure. The magnetic bearing can still suspend the rotor without contact when some of the power amplifiers fail.

The reliability of the magnetic bearings is system specific for two reasons. (a) An exact solution CDM may not exist for certain pole failure combinations. An approximate solution will always exist though and its effectiveness is evaluated via failure simulation for the specific system studied. (b) The success criterion is defined by: no contact between the shaft and catcher bearings during the failure and CDM implementation sequence. Satisfaction of this criterion will depend on the system studied and the delay time τ_d required to identify which poles have failed, to turn off the power amplifiers for these poles, and to implement the corresponding CDM for the remaining poles.

Let R_p represent the reliability of a "pole", i.e. of the power amplifier plus its pole coil, at some specific point in its expected lifetime. Also assume that "poles" are identical and act independently. The system reliability then becomes

$$R_{sys} = \sum_{k=m}^{n} \alpha_k R_p{}^k (1 - R_p)^{n-k} \tag{2.54}$$

where α_k are the number of cases which satisfy the success criterion when k poles work. The integer m in (2.54) is the minimum number of unfailed poles that are required for the n pole bearing to successfully levitate the shaft.

2.6 Examples and Simulations

2.6.1 Module Info

Table 2.1 Flywheel Model Parameter List.

Parameter	Value	Parameter	Value
m_r	29.644 (kg)	m_h	34.428 (kg)
I_{tr}	0.26233 (kg-m^2)	I_{pr}	0.11129 (kg-m^2)
I_{t1h}	1.5337 (kg-m^2)	I_{t2h}	1.3993 (kg-m^2)
K_e	3.5024E+5 (N/m)	C_e	5.2535E+3 (kg/s)
ω	60,000 (rpm)	e	8.4667E-7 (m)
L_{br}^A	0.14051 (m)	L_{br}^B	0.13360 (m)
L_{dr}^A	0.14051 (m)	L_{dr}^B	0.13360 (m)
L_{sr}^A	0.17846 (m)	L_{sr}^B	0.16974 (m)
L_{cr}^A	0.26765 (m)	L_{cr}^B	0.28067 (m)
L_{bh}^A	0.14051 (m)	L_{bh}^B	0.13360 (m)
L_{sh}^A	0.17856 (m)	L_{sh}^B	0.16974 (m)
L_{ch}^A	0.26765 (m)	L_{ch}^B	0.28067 (m)
L_{eh}^A	0.26765 (m)	L_{eh}^B	0.28067 (m)
ψ	$\pi / 2$		

An example flywheel module illustrates the FTC operation and reliability of the redundant magnetic suspension. Table 2.1 lists the geometrical, inertia, and stiffness parameters for the model. The catcher bearing contact model in Fig. 2.5 has a stiffness of 10^8 N/m, a damping of 5,000 N-s/m, and a dynamic friction coefficient of 0.1. Table 2.2 shows the magnetic bearing parameters for the magnetic suspension model. The inductance matrix of the combo bearing with the two de-coupling chokes is given in henries as

$$L_{CB} = 5.59\times10^{-4}\cdot diag(1 \quad 1 \quad 1 \quad 1 \quad 1 \quad 1 \quad 10.43 \quad 10.43)$$

The inductance matrix of the radial bearing with a de-coupling choke is given in henries as

$$L_{RB} = 6.76\times10^{-4}\cdot diag(1 \quad 1 \quad 1 \quad 1 \quad 1 \quad 1)$$

Table 2.2 Magnetic Bearing Parameter List.

Parameter	Combo Bearing	Radial Bearing
air gap	radial: 5.080E-4 (m) axial: 5.080E-4 (m)	Radial: 5.080E-4 (m) dead pole: 2.030E-3 (m)
radial pole face area	3.924E-4 (m^2)	4.764E-4 (m^2)
axial pole face area	1.719E-3 (m^2)	N/A
dead pole face area	N/A	4.962E-3 (m^2)
total face area of PM	3.178E-3 (m^2)	3.844E-3 (m^2)
length of PM	0.010 (m)	0.010 (m)
no. of turns of radial coil	24	24
no. of turns of axial coil	37	N/A
relative permeability of PM	1.055	1.055
coercive force of PM	950000 (A/m)	950000 (A/m)

The remaining parameters of the system model include displacement sensor sensitivity of 7874 V/m, displacement sensor bandwidth of 5000 Hz, power amplifier DC gain of 1 A/V, and power amplifier bandwidth of 1200 Hz.

2.6.2 Flux Leakage and Fringing Effect

The 1D magnetic circuit models as shown in Figs. 2.2 and 2.3 must be adjusted to include the effects of recirculation leakage of the flux between the N and S poles of any permanent magnet and for the effect of non-parallel (fringing) flux flow in the air gap of each pole. These effects are apparent in a 3D finite element based simulation of the actuator as shown in Fig. 2.7. These adjustments are made with multiplicative factors applied to the gap flux and permanent magnetic coercive force in the 1D model, as derived from the 3D FE model. The permanent magnet coercive force is de-rated from 950,000 A/m to 514,000 A/m in the combo bearing and from 950,000 A/m to 566,000 A/m in the radial bearing. The air gap fluxes are de-rated with a fringe factor of 0.9 for both the combo and radial bearings.

These 3D bearing models were also employed to verify the fault tolerant operation predicted with the 1D model. An example of this is the 3 pole failure results shown in Table 2.3. The control voltage sets in this table are

$$V_c = \begin{pmatrix} V_{c1} & V_{c2} & V_{c3} \end{pmatrix}^T = \begin{cases} \begin{pmatrix} 1V & 0 & 0 \end{pmatrix}^T & for \quad set \quad 1 \\ \begin{pmatrix} 0 & 1V & 0 \end{pmatrix}^T & for \quad set \quad 2 \\ \begin{pmatrix} 0 & 0 & 1V \end{pmatrix}^T & for \quad set \quad 3 \end{cases}$$

The values of 3D FE models demonstrate the linear and decoupled relation between control voltages and magnetic forces. The 1D magnetic circuit model with flux leakage and with fringing effect approximates the 3D FE models.

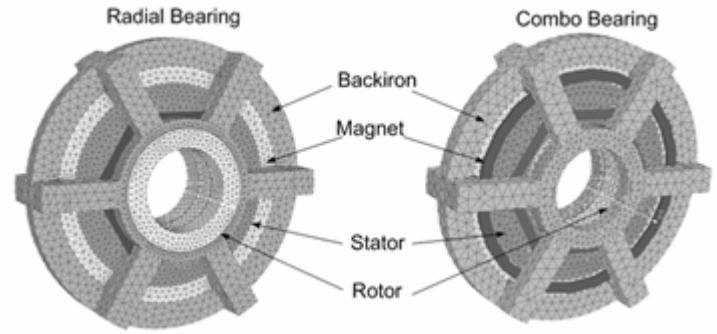

Fig. 2.7 3D FE Model of the Combo and Radial 6 Pole Actuators.

Table 2.3 1D and 3D Model Comparison of Predicted Forces for 6 Pole Combo Bearing.

Control Voltage Set	Force Direction	Force (N)			
		No Poles Failed		3 Poles Failed	
		1D Model	3D Model	1D Model	3D Model
1	X1	11.64	12.95	11.64	12.96
1	X2	0	0.01	-0.14	-0.25
1	X3	0	0.04	0	-0.03
2	X1	0	0.02	0	-0.08
2	X2	11.64	13.3	11.59	13.17
2	X3	0	0.08	0	-0.05
3	X1	0	-0.4	0	-0.4
3	X2	0	0.66	0	0.66
3	X3	8.9	9.4	8.9	9.4

2.6.3 CDMs of Six Pole HCB and HRB

According to Section 2.1, the CDMs can be obtained for different failure combinations. The following CDMs of Six Pole HCB and HRB are utilized in the simulations.

The CDMs for unfailed state are

$$T_o^A = \begin{bmatrix} 0.30789 & 0.17776 & 0 \\ 0 & 0.35552 & 0 \\ -0.30789 & 0.17776 & 0 \\ -0.30789 & -0.17776 & 0 \\ 0 & -0.35552 & 0 \\ 0.30789 & -0.17776 & 0 \\ 0 & 0 & -0.11530 \\ 0 & 0 & 0.11530 \end{bmatrix} \text{ and } T_o^B = \begin{bmatrix} 0.28074 & 0.16209 \\ 0 & 0.32417 \\ -0.28074 & 0.16209 \\ -0.28074 & -0.16209 \\ 0 & -0.32417 \\ 0.28074 & -0.16209 \end{bmatrix}$$

The new CDMs for the poles 1-2 failed case are

$$T_{12}^A = \begin{bmatrix} 0 & 0 & 0 \\ 0 & 0 & 0 \\ -0.66389 & 0 & 0 \\ -0.23032 & -0.58296 & 0 \\ -0.38545 & -0.48360 & 0 \\ 0.33734 & -0.57934 & 0 \\ 0 & 0 & -0.11530 \\ 0 & 0 & 0.11530 \end{bmatrix} \text{ and } T_{12}^B = \begin{bmatrix} 0 & 0 \\ 0 & 0 \\ -0.60475 & 0 \\ -0.21182 & -0.53041 \\ -0.34967 & -0.44211 \\ 0.30640 & -0.52769 \end{bmatrix}$$

The new CDMs for the poles 1-2-3-4 failed case are

$$T_{1234}^{A}=\begin{bmatrix} 0 & 0 & 0 \\ 0 & 0 & 0 \\ 0 & 0 & 0 \\ 0 & 0 & 0 \\ -0.60742 & -1.0622 & 0 \\ 1.2224 & -3.6408\times10^{-3} & 0 \\ 0 & 0 & -0.11530 \\ 0 & 0 & 0.11530 \end{bmatrix} \text{ and } T_{1234}^{B}=\begin{bmatrix} 0 & 0 \\ 0 & 0 \\ 0 & 0 \\ 0 & 0 \\ -0.55379 & -0.96848 \\ 1.11460 & -3.3556\times10^{-3} \end{bmatrix}$$

2.6.4 Fault Tolerant Control of 6 Pole HOMBs with Power Amplifier Failures

The text below discusses two illustrative examples that assume identical failures in both the radial and combo bearings. Although this represents a rare occurrence it serves to illustrate the method and analysis presented. Example 1 considers failing radial poles 1 and 2, and example 2 considers failing radial poles 1, 2, 3, and 4 in Fig. 2.1.

Figure 2.8 reveals that for example 1 excellent control is maintained utilizing the CDMs for no-pole failed state throughout the entire simulation. This example shows that the closed loop is still stable due to the partial actuator failure. The currents in the 14 amplifiers are shown in Figs. 2.9 and 2.10 for a failure initiation at 0.1 s. The currents of the failed PAs become zero, and the currents of the unfailed PAs are the same as before failure. Consequently the no-poles failed CDMs satisfy the success criterion for the reliability and are independent of the delay time.

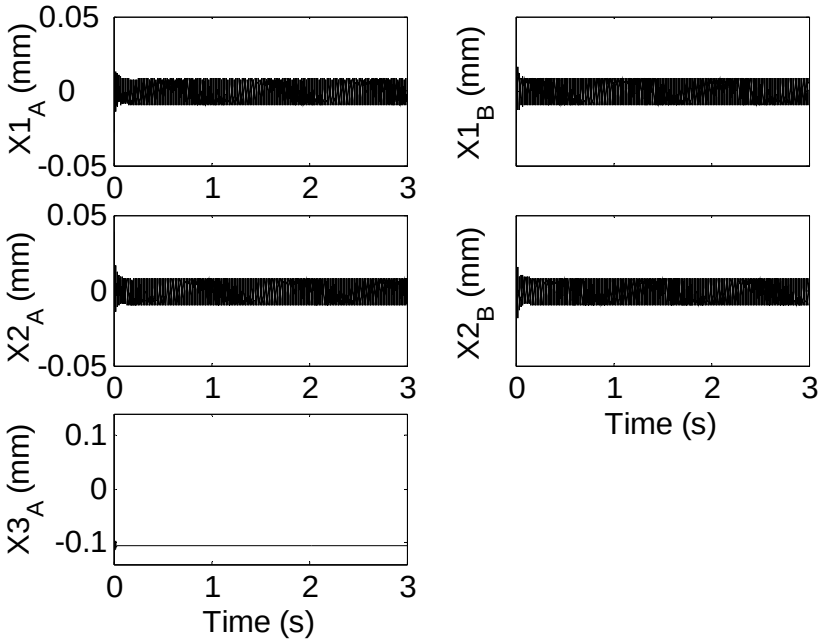

Fig. 2.8 Rotor Displacements in the Radial and Axial Directions for Example 1.

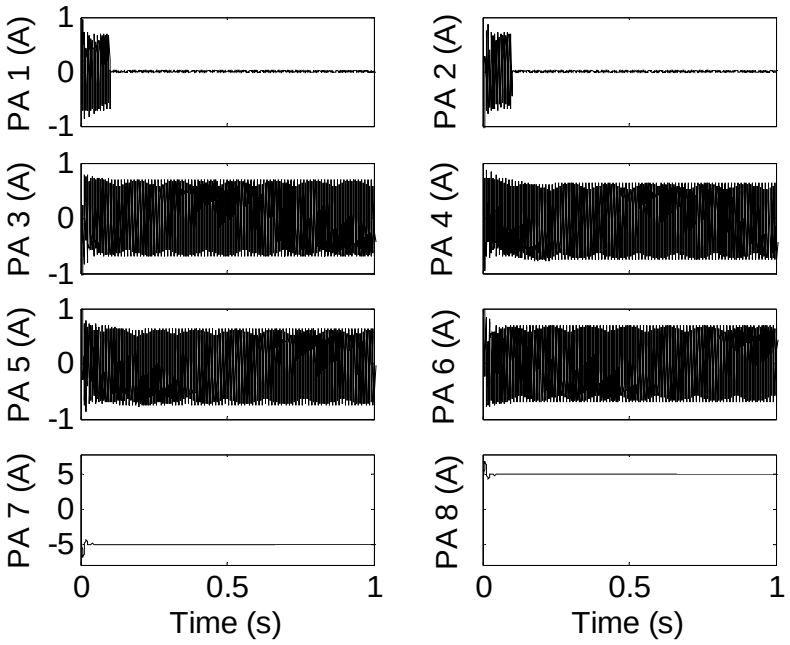

Fig. 2.9 Current Responses in HCB for Example 1.

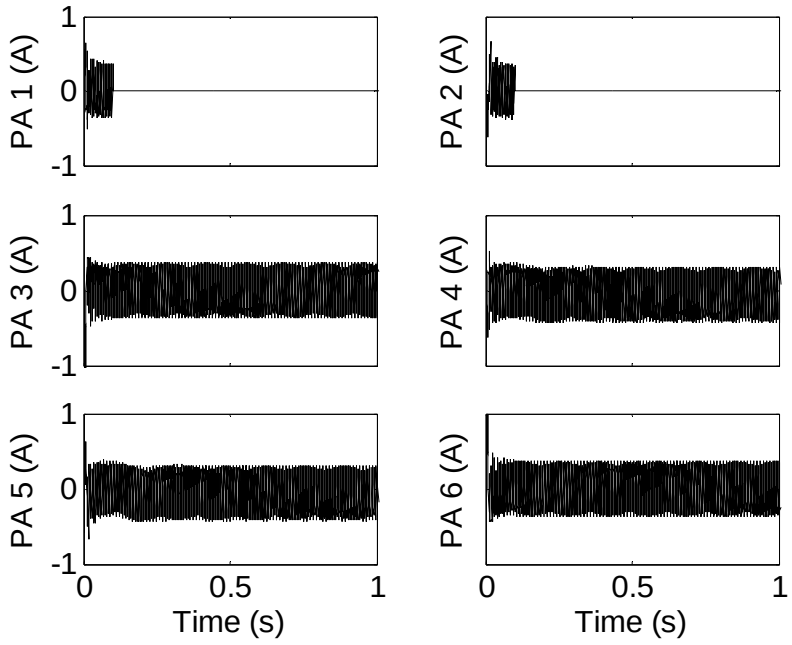

Fig. 2.10 Current Responses in HRB for Example 1.

In contrast, the closed loop system of example 2 is not stable with partial actuator failure if the CDM is not swapped. The 1-2-3-4 poles failed CDMs ($T_{1234}^{A}, T_{1234}^{B}$) must be activated after delay time to maintain control invariance. Assume that delay time τ_d = 20 ms and a failure initiation at 0.1 s.

The displacements shown in Fig. 2.11 have transient responses due to the PA failure. However they return to steady state after the new CDMs are activated. The current responses are shown in Figs. 2.12 and 2.13. The currents of the failed PAs become zero after the failure, but the currents of the unfailed PAs increase due to the larger Frobenius norms of the new CDMs.

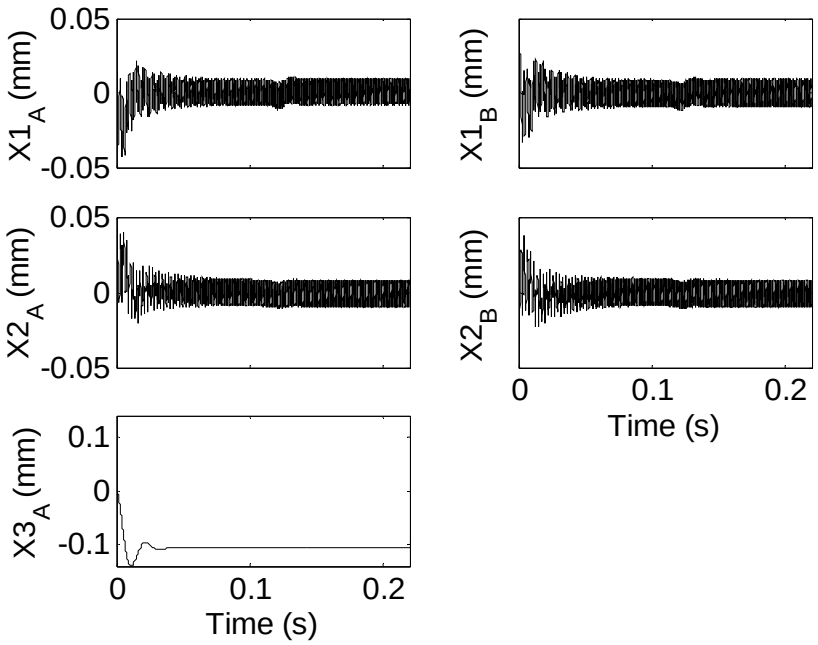

Fig. 2.11 Rotor Displacements in the Radial and Axial Directions for Example 2.

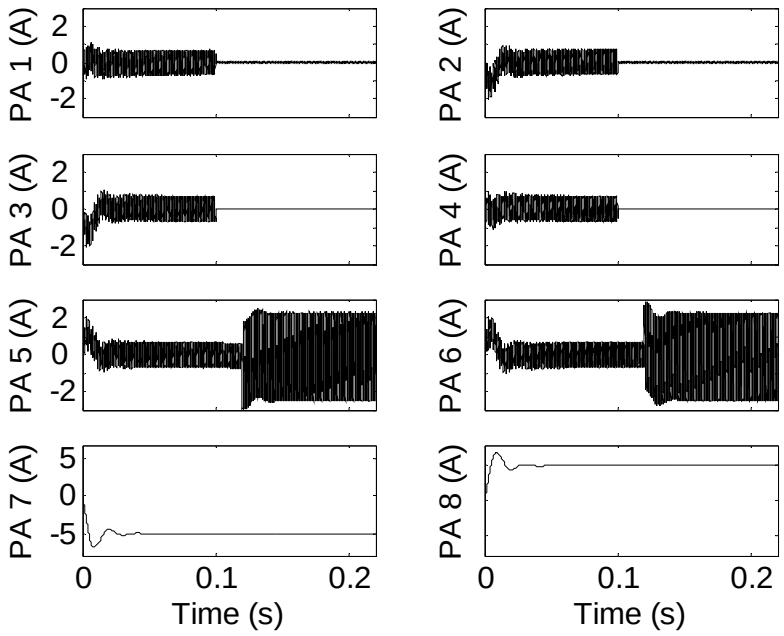

Fig. 2.12 Current Responses in HCB for Example 2.

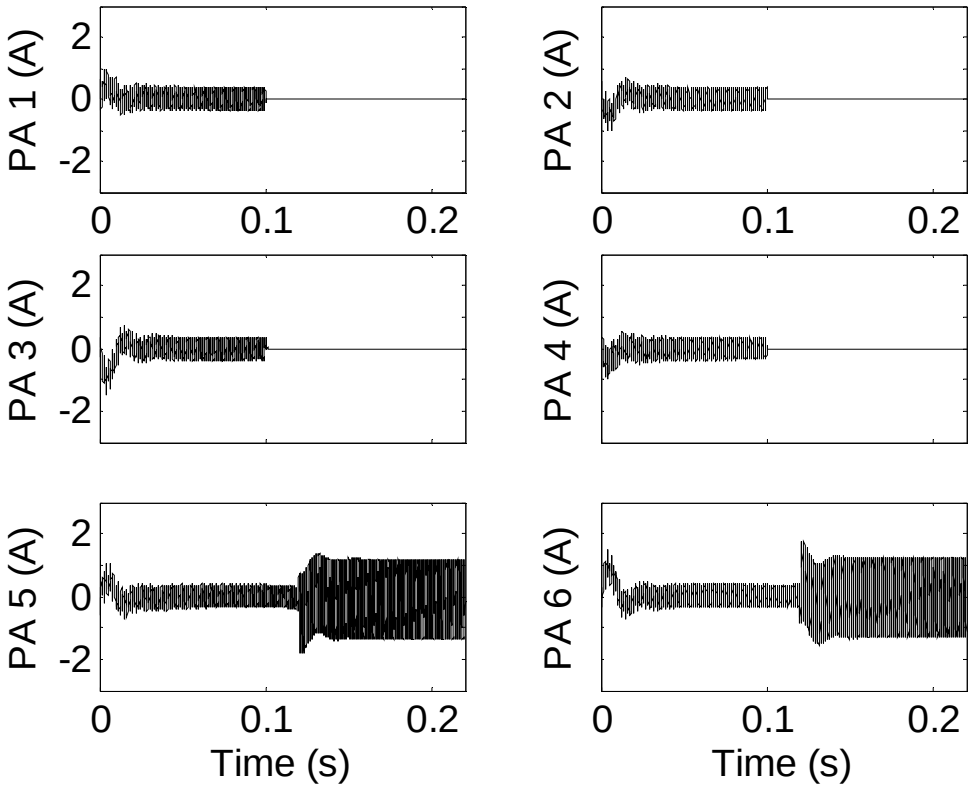

Fig. 2.13 Current Responses in HRB for Example 2.

Flux densities are shown in Figs. 2.14 and 2.15. The bias flux density in the radial poles is around 0.7 T for the HRB and 0.72 T for the HCB. The control flux of the HCB is around 0.03 T (4% of the bias flux) before the failure and 0.1 T (14% of the bias flux) after the failure. The control flux of the HRB is around 0.015 T (2% of the bias flux) before the failure and 0.05 T (7% of the bias flux) after the failure. Consequently the 1-2-3-4 poles failed CDMs satisfy the success criterion for reliability.

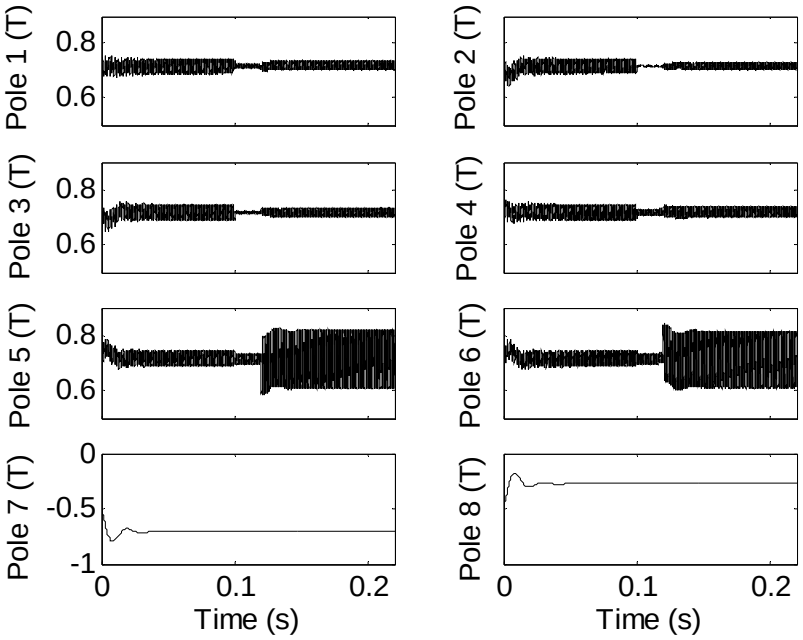

Fig. 2.14 Flux Density Responses in HCB for Example 2.

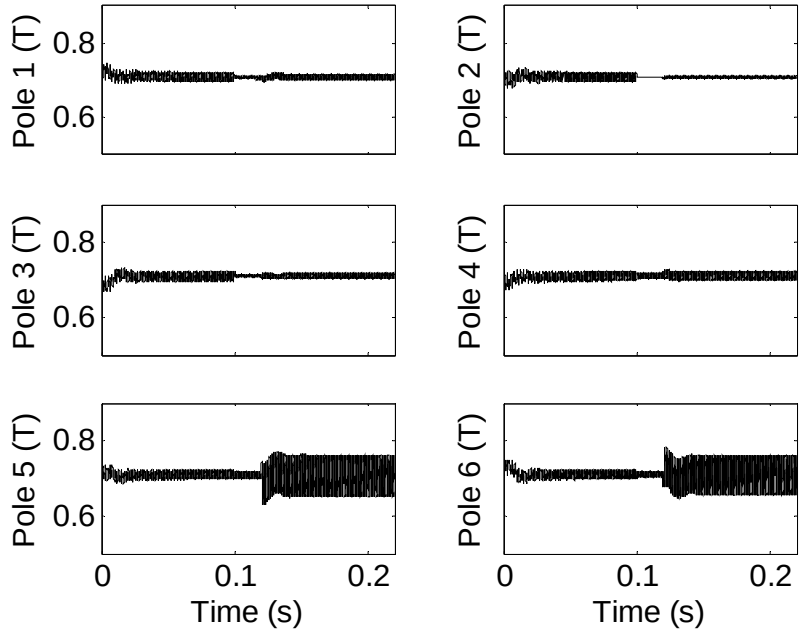

Fig. 2.15 Flux Density Responses in HRB for Example 2.

When contacts between the rotor and the catcher bearings happen during swapping the CDMs, the rotor may be re-levitated. Figure 2.16 shows the displacements for a successful re-levitation event with poles 1-2-3-4 failed, τ_d =100 ms, μ=0.1, C_c =5,000 N-s/m, and K_c =10^8 N/m.This is highly dependent on whether backward whirl develops during the contact period. The backward whirl state occurs due to friction at the contact interface between the shaft and the catcher bearings, which forces the shaft to whirl (precess) in a direction opposite to the spin direction.

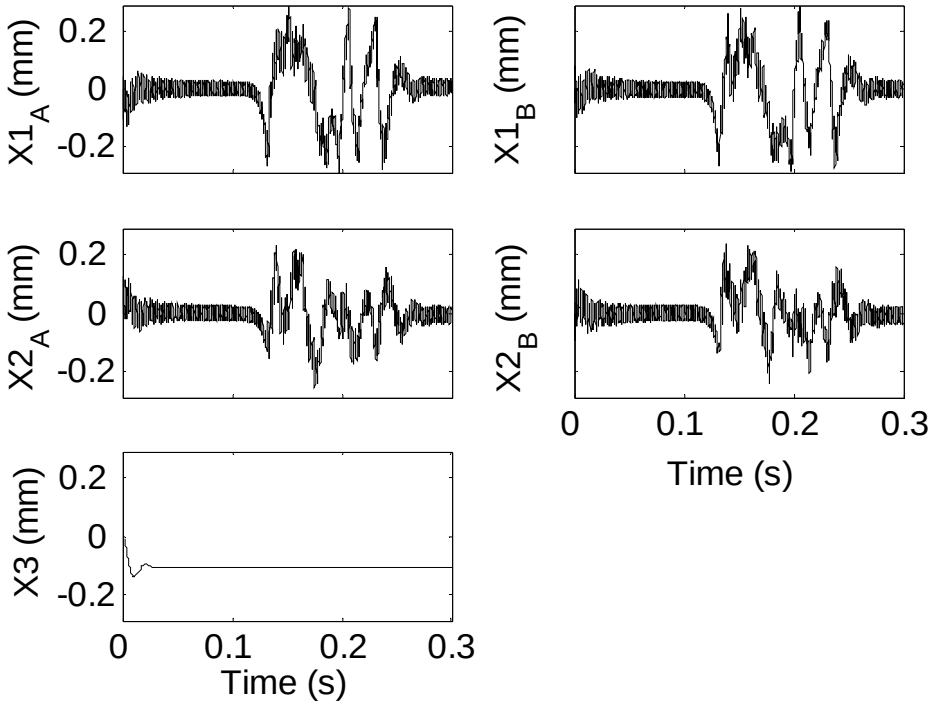

Fig. 2.16 Rotor Displacements in the Radial and Axial Directions during Successful Re-levitation.

Figure 2.17 shows an example of this state with μ=0.3, C_c =10^5 N-s/m, and K_c =10^8 N/m. The backward whirl eccentricity is the catcher bearing clearance (typically 0.25 mm) for a rigid rotor and possibly a much larger value for a flexible shaft. The whirl frequency typically ranges from 0.4-1.0 times the spin frequency. This creates a potentially large centrifugal force that can damage the catcher bearings or deflect the shaft into the magnetic bearings. The backward whirl condition is mitigated by proper design of the flexible damped support, preload, clearance, and friction coefficient for the catcher bearings. Re-levitation off of the catcher bearings is very difficult once backward whirl has fully developed.

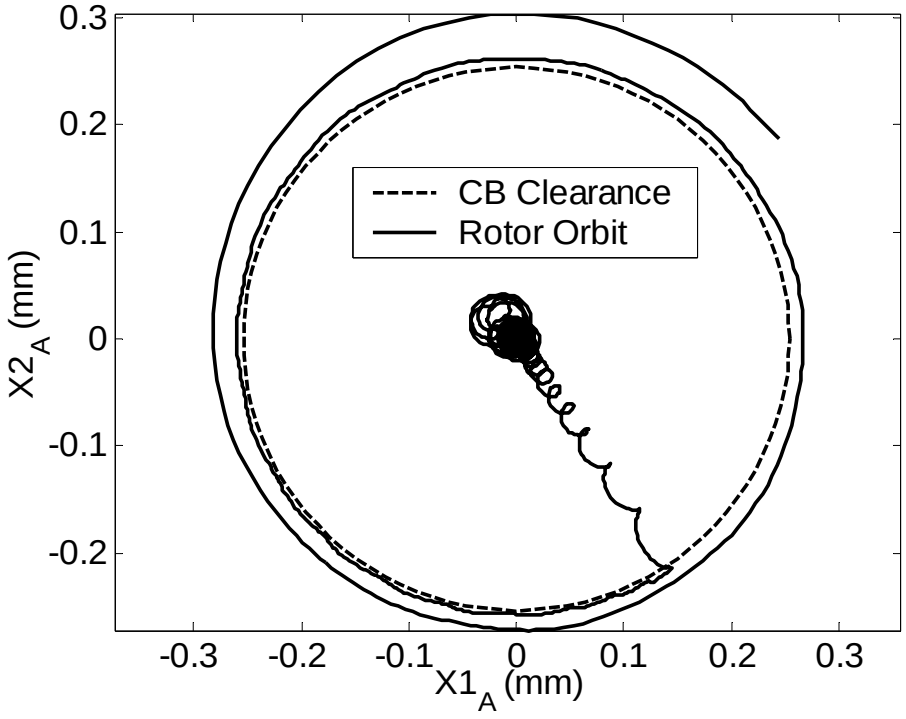

Fig. 2.17 Orbit Plot of the Rotor at CB (A).

2.6.5 Reliabilities of 4, 6, and 7 Pole HOMBs

Table 2.4 Summary of Simulation for Reliability Study.

No. of Pole	Failed Bearing	No. of unfailed Poles	No. of Simulation	Swapping CDM (α_k)	Non-Swapping CDM (α_k)
4	Radial	2	6	4	4
		3	4	4	4
		4	1	1	1
	Combo	2	6	4	4
		3	4	4	4
		4	1	1	1
6	Radial	2	15	12	0
		3	20	20	8
		4	15	15	12
		5	6	6	6
		6	1	1	1
	Combo	2	15	12	0
		3	20	20	8
		4	15	15	12
		5	6	6	6
		6	1	1	1
7	Radial	2	21	16	0
		3	35	33	0
		4	35	35	14
		5	21	21	21
		6	7	7	7
		7	1	1	1
	Combo	2	21	13	0
		3	35	28	2
		4	35	35	14
		5	21	21	20
		6	7	7	7
		7	1	1	1

The reliability of a magnetic bearing is determined by considering the number of failed pole states that still meet the success criterion. This is dependent on the delay time, modeling assumptions, number of poles in the bearing, and the reliability of the power amplifier/coil units that drive and conduct the bearing currents. The 4 pole and 7 pole configurations require 2 less or 1 more power amplifiers than the 6 pole configuration, respectively. The radial pole and permanent magnet cross-section areas, the number of turns of each radial coil, and the coercive force and the length of the permanent magnets for the 4 and 7 pole bearings are identical to those of the 6 pole bearing.

Two FTC approaches are utilized for the reliability study. The swapping CDMs approach is that the radial pole failure simulations are conducted with the combo bearing operating in a no-pole failed state, and vice versa. Failure occurs at 0.1 seconds into the simulation and swapping in of the new CDM occurs at a delay time 20 ms later. The other is the non-swapping approach, which maintains the no-pole failed CDMs. Table 2.4 summarizes the results of these simulations for swapping in the appropriate poles-failed (new) CDM and for non-swapping CDMs.

By “k-out-of-n” system structure, (2.54), and Table 2.4, Fig. 2.18 shows system reliability vs. R_p plots for the 4, 6, and 7 pole HRBs by swapping CDMs approach and for the 2-axis magnetic bearing (without redundant design, i.e. if one of the two PAs fails, the magnetic bearing fails). The HRB reliability is improved by increasing the number of radial poles and by the swapping CDMs approach even if R_p is decreasing according to the lifetime distribution. Similarly, Fig. 2.19 is for the non-swapping CDM

approach (maintain the no-poles failed CDMs). The reliabilities are also dependent on the system control robustness. Increasing the number of poles does not imply higher system reliability if the CDMs are not swapped. The reliability of the swapping CDMs approach is better than the non-swapping approach under the same MIMO control law. Consequently the HCBs have the same trend as HRBs have.

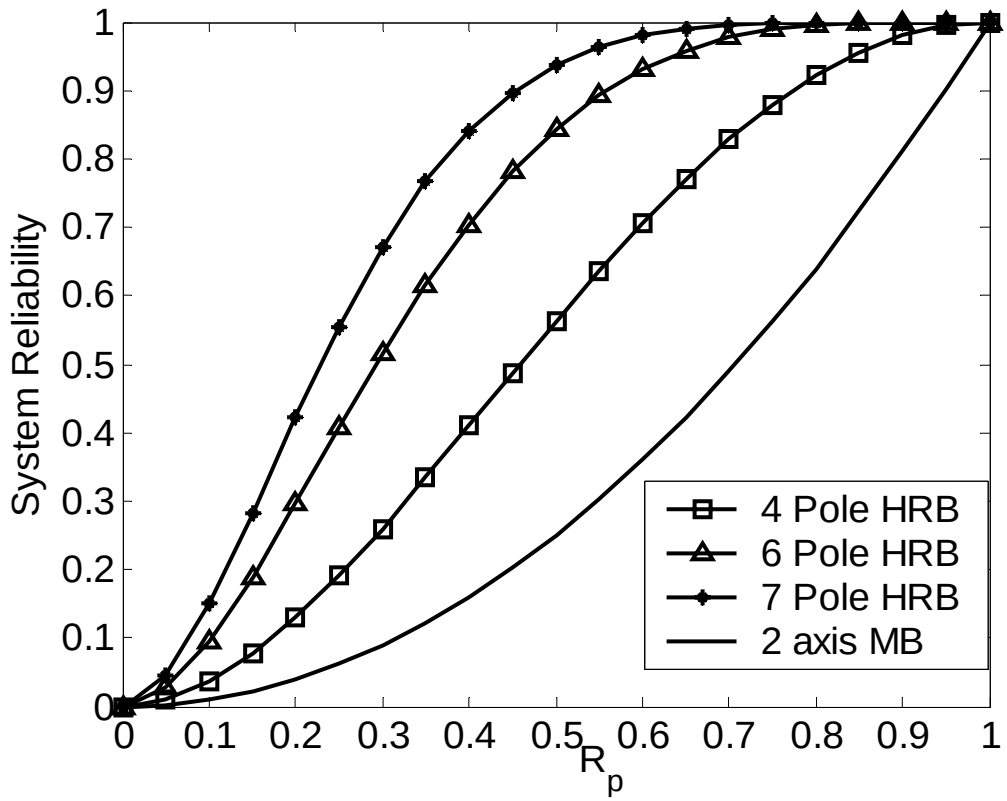

Fig. 2.18 System Reliabilities of 4, 6, and 7 Pole Radial Bearings for Swapping CDMs.

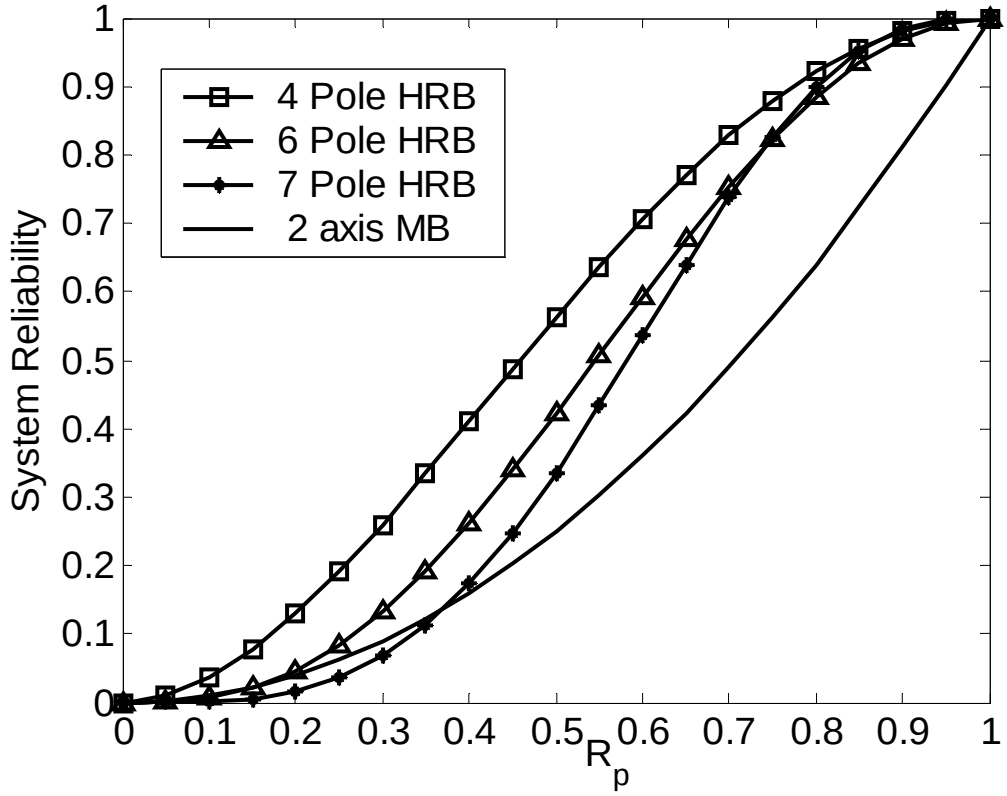

Fig. 2.19 System Reliabilities of 4, 6, and 7 Pole Radial Bearings for Non-Swapping CDMs.

CHAPTER III

FAULT-TOLERANT CIRCULAR SENSOR ARRAYS

Sensor runout is a major disturbance in rotating machinery supported on magnetic bearing systems. A circular sensor array with weighting gain matrix (WGM) is presented which can eliminate higher harmonics of runout even with failed sensors. Two criteria for sensor array failure and runout reduction are defined for evaluating the sensor array reliability based on uncoupling x_1 and x_2 sensing and runout reduction. In general, the reliability and runout reduction increase as the number of sensors increase. The array reliability and runout reduction that results by updating the WGM after a sensor failure is shown to be better than without updating. The methodology is demonstrated by a simulation of an energy storage flywheel system.

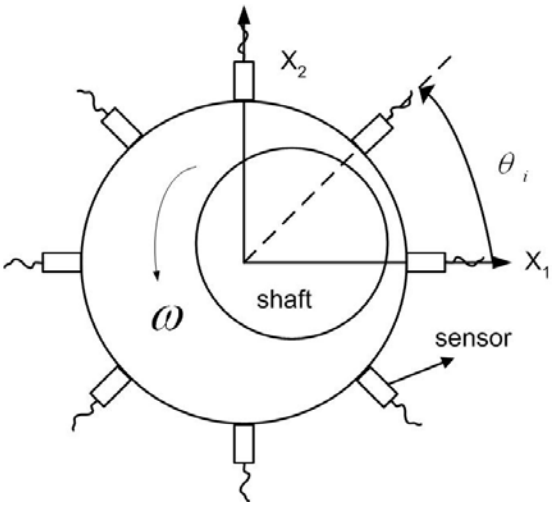

Fig. 3.1 Sensor Array with 8 Sensors.

3.1 Weighting Gain Matrix

Figure 3.1 illustrates an 8 sensor array with equal angular spacing around the circumference of the shaft. The shaft can move in either the x_1 or x_2 directions and spins at frequency ω. The objectives of the sensor array are to produce voltages proportional to x_1 and x_2, which are free from cross-coupling between the two directions and from false motions due to shaft runout.

3.1.1 Shaft Centerline Displacement Measurements

The sensor array output is a weighted sum of all sensor output signals in the array. The objective is to provide a reliable measurement of the shaft centerline radial position even if some of the sensors fail and with significant levels of runout. This is accomplished by determining an appropriate linear mapping between sensor and array outputs via a WGM. Assume that the array has n independent, identical sensors that have sensor sensitivity, ξ V/m. Then the WGM is the 2-by-n T matrix defined in the relation

$$V_s = \begin{bmatrix} v_{s1} \\ v_{s2} \end{bmatrix} = \xi TF \begin{bmatrix} d_1 \\ \vdots \\ d_n \end{bmatrix} \tag{3.1}$$

where F is an n-by-n diagonal matrix which indicates the failure configuration of the array. The entries in matrix F are binary state: F_{ii}=1 (unfailed) or F_{ii}=0 (failed). The symbol d_i in (3.1) represents the displacement measurement along the direction of the ith sensor, and v_{s1} and v_{s2} are the array outputs which correspond to the two transverse displacements (x_1 and x_2) of the shaft. Each sensor measurement can be expressed in terms of the shaft displacements

$$\begin{bmatrix} d_1 \\ \vdots \\ d_n \end{bmatrix} = \begin{bmatrix} \cos\theta_i & \sin\theta_i \\ \vdots & \vdots \\ \cos\theta_n & \sin\theta_n \end{bmatrix} \begin{bmatrix} x_1 \\ x_2 \end{bmatrix} = \Theta X \tag{3.2}$$

where θ_i is the angle between the ith sensor and axis x_1. By combining (3.2) into (3.1), the array outputs in terms of shaft centerline displacements become

$$V_s = \xi TF\Theta X \tag{3.3}$$

The constraint from (3.3)

$$TF\Theta = I \tag{3.4}$$

must be satisfied to maintain invariance between shaft motions and the array outputs in the presence of sensor failures, where I is the 2-by-2 identity matrix. Then there are 4 linear constraint equations on the T_{ij} given as

$$\sum_{i=1}^{n} \cos(\theta_i) T_{1i} F_{ii} - 1 = 0 \tag{3.5}$$

$$\sum_{i=1}^{n} \sin(\theta_i) T_{1i} F_{ii} = 0 \tag{3.6}$$

$$\sum_{i=1}^{n} \cos(\theta_i) T_{2i} F_{ii} = 0 \tag{3.7}$$

$$\sum_{i=1}^{n} \sin(\theta_i) T_{2i} F_{ii} - 1 = 0 \tag{3.8}$$

3.1.2 Sensor Runout Effect

The runout sensed by the ith sensor is expressed as the Fourier series expansion

$$\begin{aligned} g_i(t) &= \sum_{k=0}^{\infty}[a_k \cos(k\omega t - k\theta_i) + b_k \sin(k\omega t - k\theta_i)] \\ &= \sum_{k=0}^{\infty}\sqrt{a_k{}^2 + b_k{}^2}[\cos(k\omega t - \phi_k)\cos(k\theta_i) + \sin(k\omega t - \phi_k)\sin(k\theta_i)] \end{aligned} \tag{3.9}$$

where k is the number of runout harmonics, a_k and b_k are Fourier coefficients, ω is the shaft spin frequency, and

$$\phi_k = \tan^{-1}(b_k / a_k) \tag{3.10}$$

Similar to (3.1) the sensor array outputs due solely to runout are

$$V_r = \begin{bmatrix} v_{r1} \\ v_{r2} \end{bmatrix} = \xi TF \begin{bmatrix} g_1 \\ \vdots \\ g_n \end{bmatrix} \tag{3.11}$$

Substitution of (3.9) into (3.11) yields

$$v_{rj} = \sum_{k=0}^{\infty}\xi\sqrt{a_k{}^2 + b_k{}^2}\gamma_{jk}\cos(k\omega t - \phi_k - \psi_{jk}) \quad \text{j=1, 2} \tag{3.12}$$

where

$$\gamma_{jk} = \sqrt{\left(\sum_{i=1}^{n}\cos(k\theta_i)T_{ji}F_{ii}\right)^2 + \left(\sum_{i=1}^{n}\sin(k\theta_i)T_{ji}F_{ii}\right)^2} \quad \text{j=1, 2} \tag{3.13}$$

$$\psi_{jk} = \tan^{-}\left(\frac{\sum_{i=1}^{n}\sin(k\theta_i)T_{ji}F_{ii}}{\sum_{i=1}^{n}\cos(k\theta_i)T_{ji}F_{ii}}\right) \quad \text{j=1, 2} \tag{3.14}$$

From (3.12), the kth harmonic of runout is eliminated from the array's jth output if γ_{jk} is zero. Thus from (3.12) and (3.13) to eliminate one harmonic, the 4 linear constraint equations

$$\sum_{i=1}^{n} \cos(k\theta_i) T_{ji} F_{ii} = 0 \quad \text{j=1, 2} \tag{3.15}$$

$$\sum_{i=1}^{n} \sin(k\theta_i) T_{ji} F_{ii} = 0 \quad \text{j=1, 2} \tag{3.16}$$

must be satisfied. Note that for the 1st harmonic (k=1) of runout, (3.15) and (3.16) become

$$\sum_{i=1}^{n} \cos(\theta_i) T_{1i} F_{ii} = 0 \tag{3.17}$$

$$\sum_{i=1}^{n} \cos(\theta_i) T_{2i} F_{ii} = 0 \tag{3.18}$$

$$\sum_{i=1}^{n} \sin(\theta_i) T_{1i} F_{ii} = 0 \tag{3.19}$$

$$\sum_{i=1}^{n} \sin(\theta_i) T_{2i} F_{ii} = 0 \tag{3.20}$$

Equations (3.17) and (3.20) contradict (3.5) and (3.8) respectively which means the fundamental harmonic of runout cannot be eliminated by the sensor array, without destroying the output invariance.

Next consider harmonics 2 to k with n_r unfailed sensors. There exists 4k constraint equations (3.5-3.8, 3.15 and 3.16 for harmonics 2 to k). Arrange these constraint equations in the matrix forms

$$AX_j = B_j \quad \text{j=1, 2} \tag{3.21}$$

where

$$A = \begin{bmatrix} \cos(\theta_1) & \cdots & \cos(\theta_n) \\ \sin(\theta_1) & \cdots & \sin(\theta_n) \\ \vdots & \vdots & \vdots \\ \cos(k\theta_1) & \cdots & \cos(k\theta_n) \\ \sin(k\theta_1) & \cdots & \sin(k\theta_n) \end{bmatrix}_{2k \times n_r} \tag{3.22}$$

$$X_j = \begin{bmatrix} T_{j1} & \cdots & T_{jn} \end{bmatrix}^T \tag{3.23}$$

$$B_1 = \begin{bmatrix} 1 & 0 & \cdots & 0 \end{bmatrix}^T \tag{3.24}$$

$$B_2 = \begin{bmatrix} 0 & 1 & 0 & \cdots & 0 \end{bmatrix}^T \tag{3.25}$$

Equation (3.21) is two de-coupling linear systems of equations with n_r unknowns (X_j). The linear systems may be over-determined ($2k>n_r$), determined ($2k=n_r$), or under-determined ($2k<n_r$). If the linear system is consistent (at least one exact solution), there is a unique solution with a minimum-norm of X_j. If the linear system is inconsistent (no exact solution), the norm of the residual vector (AX_j-B_j) can is minimized, however the solution is not unique unless the matrix A has full column rank [30].

A WGM is calculated to satisfy the constraint equations exactly or approximately for each failure configuration. There exist (2^n-1) failure combinations for an array with n sensors. Let the n sensors be equally spaced

$$\theta_i = (i-1)2\pi / n \quad \text{i=1, 2, …, n}$$

and refer to the first n harmonics of runout as the fundamental set. Then the second set (harmonics n+1 to 2n) has the same constraint equations as the fundamental set and so on. In addition,

$$\cos(n\theta_i) = 1 \tag{3.26}$$

$$\sin(n\theta_i) = 0 \tag{3.27}$$

$$\cos[(n-j)\theta_i] = \cos(j\theta_i) \tag{3.28}$$

$$\sin[(n-j)\theta_i] = -\sin(j\theta_i) \tag{3.29}$$

The matrix A in (3.22) that considers the fundamental set becomes

$$A = \begin{bmatrix} \cos(\theta_1) & \cdots & \cos(\theta_n) \\ \sin(\theta_1) & \cdots & \sin(\theta_n) \\ \cos(2\theta_1) & \cdots & \cos(2\theta_n) \\ \sin(2\theta_1) & \cdots & \sin(2\theta_n) \\ \vdots & \vdots & \vdots \\ \cos(2\theta_1) & \cdots & \cos(2\theta_n) \\ -\sin(2\theta_1) & \cdots & -\sin(2\theta_n) \\ \cos(\theta_1) & \cdots & \cos(\theta_n) \\ -\sin(\theta_1) & \cdots & -\sin(\theta_n) \\ 1 & \cdots & 1 \\ 0 & \cdots & 0 \end{bmatrix}_{2n\times n_r} \tag{3.30}$$

The constraint equations for the (n-1)th harmonic contradict (3.5) and (3.8). This also implies that the 1st and (n-1)th harmonics of runout cannot be eliminated in the fundamental set and in their corresponding harmonics in other sets. So a sensor array with n sensors located with equal angles can eliminate harmonics of runout from 2 to n-2 in the fundamental set and their corresponding harmonics in other sets. For example, an

array with 4 sensors can eliminate even harmonics, and an array with 8 sensors can eliminate harmonics 2 to 6, harmonics 10 to 14 and so on.

3.2 Sensor Array Failure Criterion and Runout Reduction Criterion

Since all of the constraint equations maynot be completely satisfied for the over-determined systems, some errors will exist in (3.5)-(3.8). Well designed control systems can tolerate measurement errors depending on the level of robustness. The sensor array failure criterion is defined based on the controller robustness limits. In practice this is quantified by considering variation of the sensor array outputs resulting from a myriad of sensor failure configurations. A measure of the error in array output invariance is obtained from (3.4) as

$$E = TF\Theta - I \tag{3.31}$$

The array is considered successful if

$$\left|E_{ij}\right| \le \delta_{ij}, \quad \text{i= 1, 2} \quad \text{j=1,2} \tag{3.32}$$

where δ_{ij} are constants and selected by considering the robustness of the controller. If (3.32) is satisfied for a failure combination, then the array is considered unfailed, and the WGM corresponding to the failure combination is considered successful for the respective configuration of failed sensors.

The kth component of runout produced the x_j array output is zero if γ_{jk} equals zeros in (3.12) and (3.13). This condition will not always hold if a sensor, or sensors have failed. Define the user defined tolerance for successful elimination of the kth

component of runout as η. Then the array is considered successful for eliminating this component if

$$\gamma_{jk} \le \eta, \quad \text{j=1, 2} \tag{3.33}$$

If (3.33) is satisfied for a sensor failure configuration, the amplitudes of the kth harmonics of runout have been reduced at least $(1-\eta)\times 100\,\%$, and the WGM is considered successful for eliminating the kth component of runout.

3.3 Sensor Array Reliability and Runout Reduction Probability

The WGMs can be calculated for all combinations of sensor failures. A WGM is considered "successful" if (3.32) and (3.33) are satisfied for a sensor failure configuration, and the system can continuously operate by swapping in the new WGM. The sensor array reliability is similar to a "k-out-of-n: G" system structure [29]. Assume all sensors in an array can fail independently and have identical lifetime distribution, and let r_s be the reliability of a single sensor, which will decrease over its life. Then the array reliability becomes

$$R_{sys} = \sum_{i=m}^{n} \alpha_i r_s^{\,i} (1-r_s)^{n-i} \tag{3.34}$$

where α_i is the number of successful cases that pass the acceptance criterion when any i sensors works, and m is the minimum number of unfailed sensors required for the system to operate.

Similarly, the runout reduction criterion is used to decide if the runout reduction goal is achieved or not. Note that (3.32) and (3.33) must be satisfied simultaneously for

the runout reduction criterion. This is because if the array fails according to the failure criterion, then the whole system fails. The runout reduction is meaningful only when the failure criterion is passed. Thus the probability to reach the runout reduction goal for the kth harmonic of runout becomes

$$P_k = \sum_{i=m}^{n} \beta_i r_s^{\,i} (1-r_s)^{n-i} \tag{3.35}$$

where β_i is the number of successful cases that satisfy both the failure criterion and the runout reduction criterion.

Since most control systems can tolerate small measurement errors the WGM may still deliver satisfactory performance if the constraint equations (3.5-3.8, 3.15, 3.16) are not exactly satisfied. Therefore it is worth while to investigate the array reliability for the case of retaining the unfailed sensor WGM even after failure of some sensors. The "swap in approach" (SIA) replaces the existing WGM with the appropriate WGM for the actual failed sensor configuration. This approach depends on reliable detection of failed sensors which requires additional hardware. The non-swap-in approach (NSIA) retains the WGM for the no sensor failed case even if some sensors fail.

3.4 Examples and Simulations

3.4.1 Array Reliability and Runout Reduction Probability

For sake of illustration let δ_{ij}=0.2, η=0.2, $r_s \in \{0.9, 0.95, 0.99, 0.999\}$, n=8 and consider runout harmonics 2 to 6, i.e., 24 constraint equations. Consider three failure combinations: case 1 for no sensor failure, case 2 for sensor 1 failure, and case 3 for

sensor 1 and 2 failure. Table 3.1 shows that the sensor array can completely eliminate harmonics 2 to 6 for case 1 and case 2 by the SIA. The SIA yields the same degree of elimination for any one-sensor failure case. Table 3.2 compares the same variables as Table 3.1 utilizing the NSIA. Note that the runout elimination is imperfect even if just one sensor fails.

Table 3.1 γ_{1k} and γ_{2k} vs. Harmonics (SIA).

k	Case 1		Case 2		Case 3	
	γ_{1k}	γ_{2k}	γ_{1k}	γ_{2k}	γ_{1k}	γ_{2k}
1	1	1	1	1	0.981	0.885
2	0	0	0	0	0.048	0.116
3	0	0	0	0	0.063	0.152
4	0	0	0	0	0.068	0.165
5	0	0	0	0	0.063	0.152
6	0	0	0	0	0.048	0.116
7	1	1	1	1	0.981	0.885
8	0	0	2	0	1.707	0.707

Table 3.2 γ_{1k} and γ_{2k} vs. Harmonics (NSIA).

k	Case 1		Case 2		Case 3	
	γ_{1k}	γ_{2k}	γ_{1k}	γ_{2k}	γ_{1k}	γ_{2k}
1	1	1	0.75	1	0.637	0.884
2	0	0	0.25	0	0.306	0.177
3	0	0	0.25	0	0.177	0.177
4	0	0	0.25	0	0.073	0.177
5	0	0	0.25	0	0.177	0.177
6	0	0	0.25	0	0.306	0.177
7	1	1	0.75	1	0.637	0.884
8	0	0	0.25	0	0.427	0.177

Table 3.3 lists the number of successful cases for SIA and Table 3.4 for NSIA. For the failure configurations with one or two failed sensors, the SIA has more cases which satisfy the criterion when considering harmonics 2 to 6. When more than two sensors fail, no failure configurations can satisfy the criterion by both approaches.

Table 3.3 Number of Successful Cases (SIA).

	$\beta_8(\alpha_8)$	$\beta_7(\alpha_7)$	$\beta_6(\alpha_6)$
n=8	1	8	8
k=1	0	0	0
k=2	1	8	8
k=3	1	8	8
k=4	1	8	8
k=5	1	8	8
k=6	1	8	8
k=7	0	0	0
k=8	1	0	0

All other $\beta_i(\alpha_i)$ are zeros.

Table 3.4 Number of Successful Cases (NSIA).

	$\beta_8(\alpha_8)$	$\beta_7(\alpha_7)$	$\beta_6(\alpha_6)$
n=8	1	4	4
k=1	0	0	0
k=2	1	4	4
k=3	1	4	4
k=4	1	4	4
k=5	1	4	4
k=6	1	4	4
k=7	0	0	0
k=8	1	4	4

All other $\beta_i(\alpha_i)$ are zeros.

By (3.34) and (3.35) and Tables 3.3 and 3.4, Tables 3.5 and 3.6 list array reliability and runout reduction probability vs. sensor reliability. The array reliability and runout reduction probabilities for harmonics 2 to 6 by SIA are higher than those by NSIA.

Table 3.5 Sensor Array Reliability and Runout Reduction Probability vs. r_s (SIA).

	r_s =0.900	r_s =0.950	r_s =0.990	r_s =0.9990
R_{sys}	0.855620	0.957457	0.998063	0.999980
P_1	0	0	0	0
P_2	0.855620	0.957457	0.998063	0.999980
P_3	0.855620	0.957457	0.998063	0.999980
P_4	0.855620	0.957457	0.998063	0.999980
P_5	0.855620	0.957457	0.998063	0.999980
P_6	0.855620	0.957457	0.998063	0.999980
P_7	0	0	0	0
P_8	0.430467	0.663420	0.922744	0.992027

Table 3.6 Sensor Array Reliability and Runout Reduction Probability vs. r_s (NSIA).

	r_s =0.900	r_s =0.950	r_s =0.990	r_s =0.999
R_{sys}	0.621786	0.803088	0.960027	0.996000
P_1	0	0	0	0
P_2	0.621786	0.803088	0.960027	0.996000
P_3	0.621786	0.803088	0.960027	0.996000
P_4	0.621786	0.803088	0.960027	0.996000
P_5	0.621786	0.803088	0.960027	0.996000
P_6	0.621786	0.803088	0.960027	0.996000
P_7	0	0	0	0
P_8	0.621786	0.803088	0.960027	0.996000

Tables 3.7 and 3.8 list SIA and NSIA array reliability vs. number of sensors and r_s when harmonics 2 to 6 are considered in each array. Figure 3.2 shows that the SIA array reliability is better than the NSIA.

Table 3.7 Sensor Array Reliability vs. Number of Sensor and r_s (SIA).

	r_s =0.900	r_s =0.950	r_s =0.990	r_s =0.999
n=8	0.855620	0.957457	0.998063	0.999980
n=9	0.839145	0.951852	0.997780	0.999977
n=10	0.826975	0.947906	0.997589	0.999975
n=11	0.815066	0.943982	0.997398	0.999973
n=12	0.847030	0.957635	0.998214	0.999982
n=13	0.820690	0.948380	0.997742	0.999977
n=14	0.899906	0.974754	0.998998	0.999990
n=15	0.986353	0.998921	0.999998	1.000000
n=16	0.994271	0.999665	1.000000	1.000000

Table 3.8 Sensor Array Reliability vs. Number of Sensor and r_s (NSIA).

	r_s =0.900	r_s =0.950	r_s =0.990	r_s =0.999
n=8	0.621786	0.803088	0.960027	0.996000
n=9	0.645701	0.829276	0.968882	0.996988
n=10	0.736099	0.913862	0.995734	0.999955
n=11	0.736099	0.913862	0.995734	0.999955
n=12	0.728738	0.911577	0.995634	0.999954
n=13	0.724902	0.911502	0.995706	0.999955
n=14	0.737141	0.919963	0.996385	0.999963
n=15	0.730080	0.920301	0.996602	0.999966
n=16	0.741971	0.925877	0.996960	0.999970

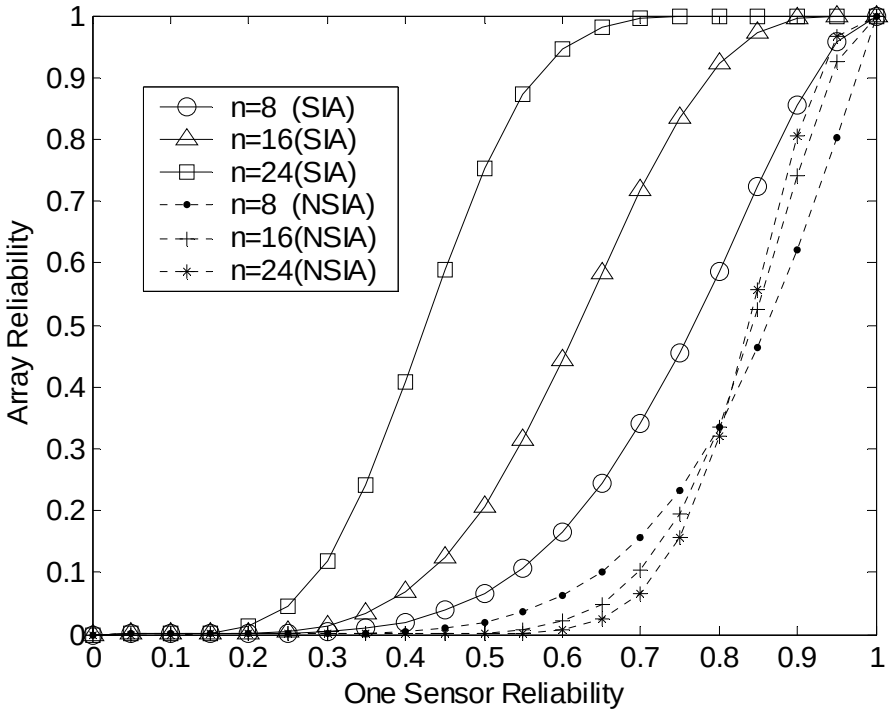

Fig. 3.2 Array Reliability vs. r_s .

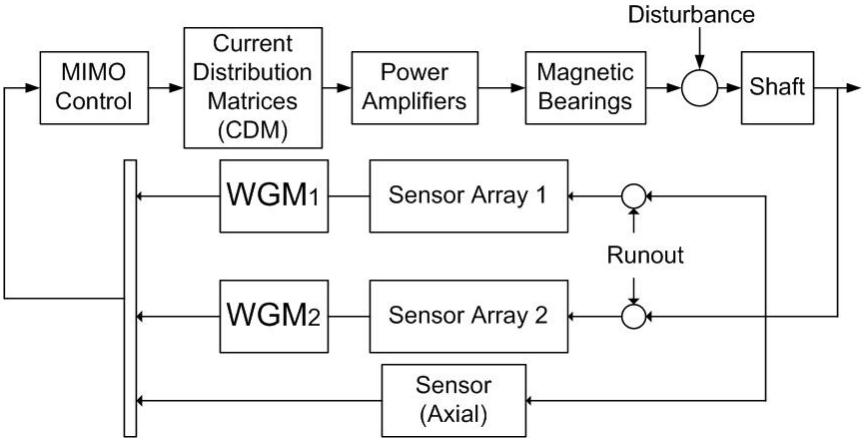

Fig. 3.3 Control Scheme with Sensor Arrays.

3.4.2 System Simulations with Sensor Failures

The flywheel-based magnetic suspension system in CHAPTER II is utilized to simulate the function of sensor arrays. The system control scheme in Fig. 3.3 uses one sensor for measuring the axial displacement and two sensor arrays: one for the axial/radial bearing and the other for the radial bearing. Each sensor in an array is represented by a 1st older filter with cut-off frequency 5 kHz and sensitivity 7874 V/m.

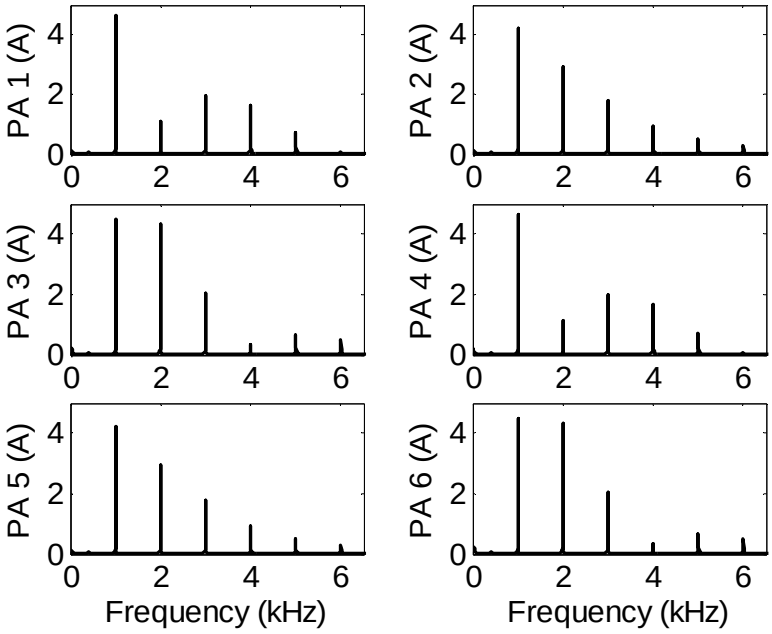

Fig. 3.4 Frequency Spectrum of Currents in HRB for n=2.

Assume that the two sensor arrays have identical sensor failure combinations and sense identical runout patterns. This results in the same runout harmonics to be reduced in all 4 outputs of the 2 sensor arrays, and consequently in the power amplifier currents.

The first 6 harmonics of runout are considered and have amplitude 0.02 mm, i.e., $a_k = b_k = 0.02$ mm.

Figure 3.4 shows the frequency spectrum of currents in the radial bearing for a two-sensor (n=2 and sensors are orthogonal) system. All harmonics of runout exist so the two-sensor system fails to eliminate the runout.

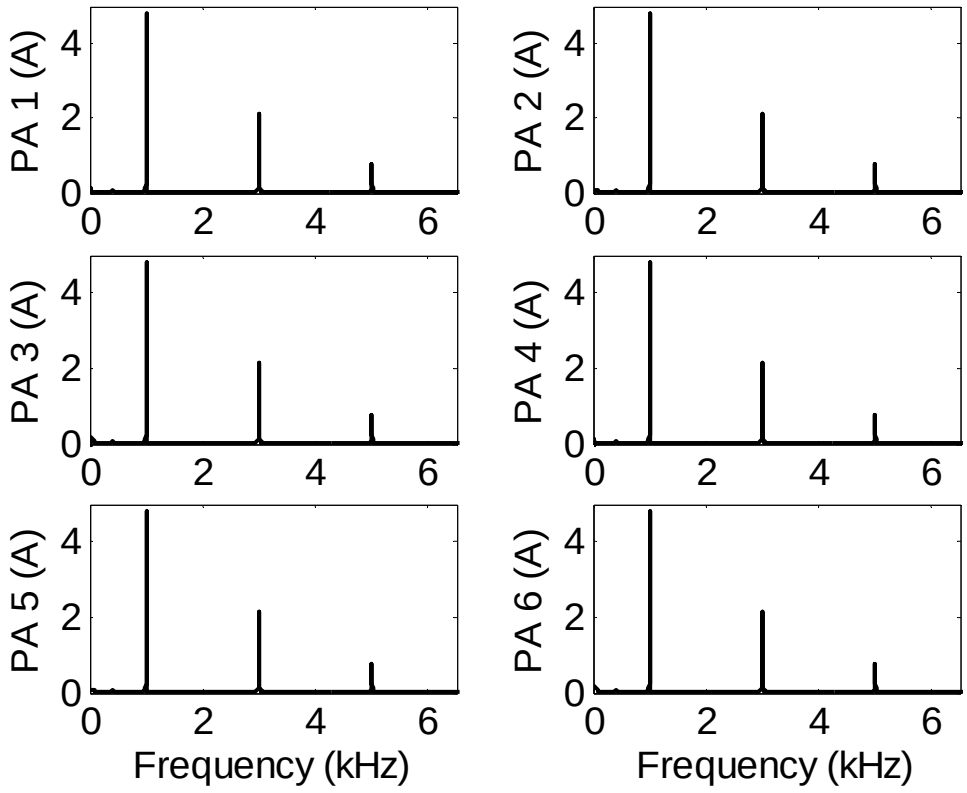

Fig. 3.5 Frequency Spectrum of Currents in HRB for n=4.

Figure 3.5 shows that for a sensor array with 4 sensors, the even harmonics are eliminated. Figure 3.6 shows that for case 1 (n=8) the higher harmonics are completely

eliminated except for the synchronous frequency. The case 2 (n=8) result is identical with case 1. Figure 3.7 is a zoomed-in range for case 3. The amplitude of the synchronous frequency in Fig. 3.7 is the same as in Fig. 3.6. The higher harmonics are not completely eliminated since the constraint equations are not completely satisfied.

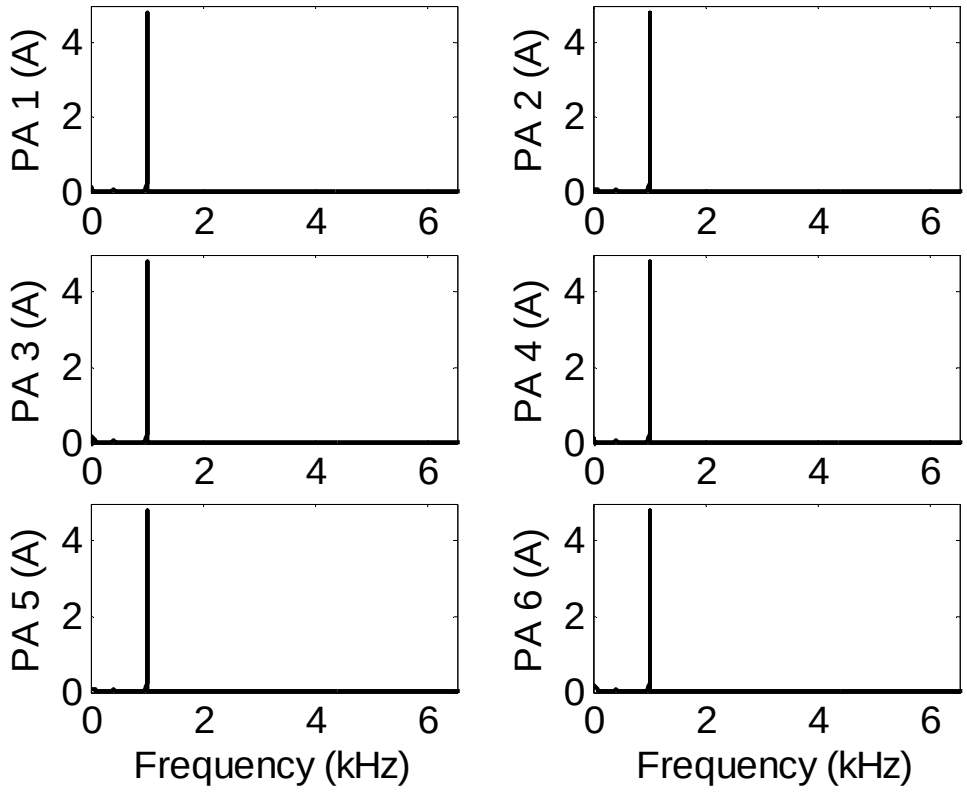

Fig. 3.6 Frequency Spectrum of Currents in HRB for Cases 1 and 2.

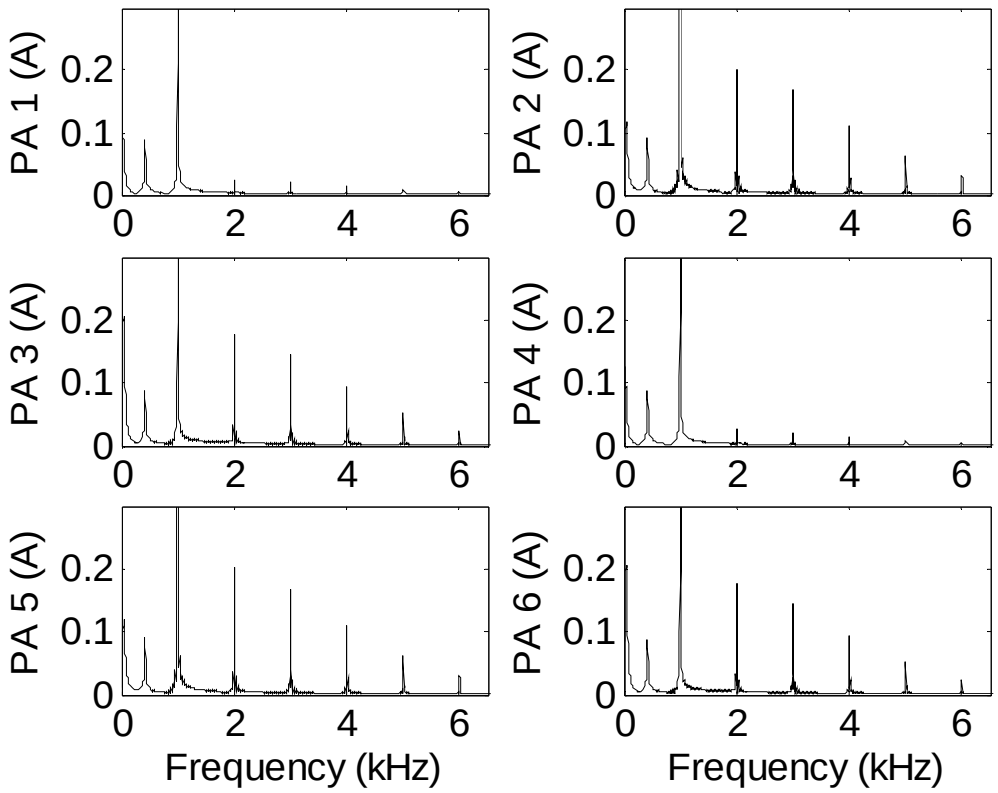

Fig. 3.7 Frequency Spectrum of Currents in HRB for Case 3 (Zoomed-in).

CHAPTER IV

ADAPTIVE CONTROL OF HOMOPOLAR MAGNETIC BEARINGS

Fault tolerant control is able to accommodate the system component faults such as the failures of actuators, sensors, and plants. Normally the operation of fault tolerant control depends on highly reliable fault detection and identification to detect the faults by the signal- or model-based approach. In this chapter, two adaptive control schemes are utilized to compensate for the actuator (power amplifier) failure in a magnetic suspension system. The gain scheduling adaptive control is combined with the signal-based fault detection to identify the failure combinations of the power amplifiers. The other scheme is that the signal-based fault detection is replaced by the model-based fault detection (estimator). The adaptive law which estimates the jump parameters in a system is derived by the Lyapunov approach. To reduce the number of persistently exciting signals, the reduced-order adaptive law is developed. The simulation results of a magnetic suspension system show that the system can continuously operate when some of the power amplifiers in a magnetic bearing fail. Thus, the reliability of a magnetic bearing is improved by the adaptive control schemes.

4.1 Simplified Dynamic Model of a Magnetic Suspension System

A simplified dynamic model which neglects the housing dynamics is shown in Fig. 4.1. The equations of motion then become

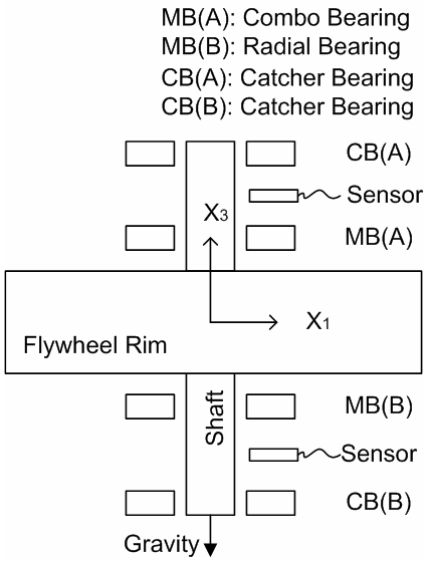

Fig. 4.1 Flywheel System with a Magnetic Suspension (Simplified).

$$M_r \ddot{X}_r + G_r \dot{X}_r = \left(T_r^{MB}\right)^T \hat{F}_{br} + \left(T_r^{CB}\right)^T \hat{F}_{cr} + B_{dr}\hat{F}_{dr} + F_{gr} \tag{4.1}$$

which is the same as in (2.36). Arrange these EOMs into state space form

$$\dot{X}_p = A_{pr} X_p + B_{pb}\hat{F}_{br} + B_{pc}\hat{F}_{cr} + B_{pd}\hat{F}_{dr} + F_g \tag{4.2}$$

where

$$X_p = \begin{bmatrix} X_r^T & \dot{X}_r^T \end{bmatrix}^T \tag{4.3}$$

$$A_{pr} = \begin{bmatrix} 0_{5\times5} & I_{5\times5} \\ 0_{5\times5} & -M_r^{-1}G_r \end{bmatrix} \tag{4.4}$$

$$B_{pb} = \begin{bmatrix} 0_{5\times5} \\ M_r^{-1}(T_r^{MB})^T \end{bmatrix} \tag{4.5}$$

$$B_{pc} = \begin{bmatrix} 0_{5\times5} \\ M_r^{-1}(T_r^{CB})^T \end{bmatrix} \tag{4.6}$$

$$B_{pd} = \begin{bmatrix} 0_{5\times 4} \\ M_r^{-1} B_{dr} \end{bmatrix} \tag{4.7}$$

$$F_g = M_r^{-1} F_{gr} \tag{4.8}$$

The linearized magnetic forces for small angle motions are given as

$$\hat{F}_{br} = K_{pmb} \hat{X}_r + K_{vmb} \hat{V}_c \tag{4.9}$$

where the matrices K_{pmb} and K_{vmb} are the position and control voltage stiffness matrices for the magnetic bearings and the vector $\hat{V}_c$ is the control voltages in the CG coordinate. The magnetic forces can also be expressed in terms of the bearing coordinate

$$\hat{F}_b = K_{pmb} T_r^{MB} X + K_{vmb} T_r^{MB} V_c \tag{4.10}$$

where the control voltage V_c is determined by the feedback control. The first term on the right-hand side of (4.10) is the magnetic forces due to the rotor displacements, which is not functions of the controller parameters. Substitution of (4.10) in (4.2) yields

$$\dot{X}_p = A_p X_p + B_p V_c + B_{pc} \hat{F}_{cr} + B_{pd} \hat{F}_{dr} + F_g \tag{4.11}$$

where

$$A_p = \begin{bmatrix} 0_{5\times 5} & I_{5\times 5} \\ M_r^{-1} \left(T_r^{MB}\right)^T K_{pmb} T_r^{MB} & -M_r^{-1} G_r \end{bmatrix} = \begin{bmatrix} 0 & I \\ A_{p21} & A_{p22} \end{bmatrix} \tag{4.12}$$

$$B_p = \begin{bmatrix} 0_{5\times 5} \\ M_r^{-1} \left(T_r^{MB}\right)^T K_{vmb} T_r^{MB} \end{bmatrix} = \begin{bmatrix} 0 \\ B_{p2} \end{bmatrix} \tag{4.13}$$

Notice that the magnetic bearings utilize the permanent magnets to supply the bias flux and the power amplifiers to supply the control flux. Then the matrix K_{pmb} will not be influenced by the power amplifier failures, but the matrix K_{vmb} will change

abruptly according to the failure combinations. In general, the matrix K_{vmb} will become un-diagonal, i.e., for the failed magnetic bearings, the control voltage for X_1 (or X_2) will influence the control force for X_2 (or X_1). In addition, the diagonal terms will decrease. The abrupt change of the matrix K_{vmb} acts like jump parameters and may cause the closed loop to be unstable, especially for more failed power amplifiers in a magnetic bearing. The following adaptive control schemes are utilized to accommodate the power amplifier failure (jump parameter).

4.2 Gain Scheduling Adaptive Control

If the signal-based fault detection is utilized to identify the failures of power amplifiers, the matrices B_{p2} for different failure combinations can be obtained in advance. The PD gains for different failure combinations can also be obtained by the following control law and are saved in a look-up table. The gain scheduling adaptive control scheme is shown in Fig. 4.2.

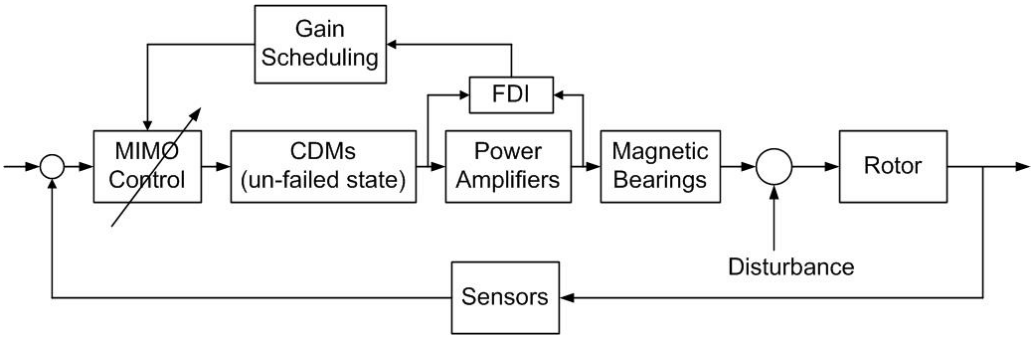

Fig. 4.2 Gain Scheduling Adaptive Control Scheme.

Assume that the feedback control law is given as

$$V_c = -K_{fb}X_p + r = -\lfloor K_{fb_1} \quad K_{fb2} \rfloor X_p + r \tag{4.14}$$

where the matrix K_{fb} is the feedback gains and the vector r is the reference signals. The closed loop system matrix becomes

$$A_{pcl} = \begin{bmatrix} 0 & I \\ A_{p21} - B_{p2}K_{fb_1} & A_{p22} - B_{p2}K_{fb2} \end{bmatrix} \tag{4.15}$$

Let the desired closed loop system matrix have the following form

$$A_t = \begin{bmatrix} 0 & I \\ A_{t21} & A_{t22} \end{bmatrix} \tag{4.16}$$

where A_{t21} and A_{t22} are negative definite, constant matrices or A_t is a stable constant matrix. Then the feedback gains become

$$K_{fb1} = B_{p2}^{-1}(A_{p21} - A_{t21}) \tag{4.17}$$

$$K_{fb2} = B_{p2}^{-1}(A_{p22} - A_{t22}) \tag{4.18}$$

By (4.17) and (4.18), the feedback gains for different failure combinations can be calculated in advance.

4.3 Adaptive Pole Placement Control

The adaptive pole placement control (APPC) scheme is shown in Fig. 4.3. For APPC, the first step is to estimate the plant parameters. If the matrices A_p and B_p are unknown, the adaptive law in [31] can be utilized. The parameter convergence is guaranteed by persistent excitation.

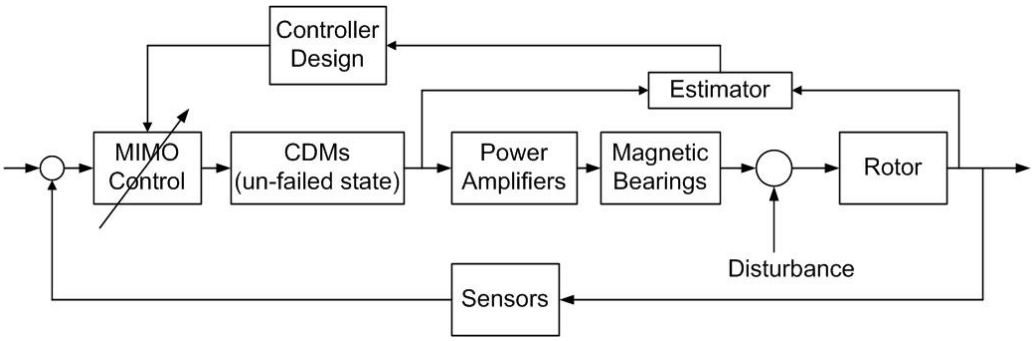

Fig. 4.3 Adaptive Pole Placement Control Scheme.

If some of the parameters are known, the order of the adaptive law and the number of persistently exciting signals can be reduced. Assume that the matrix A_p is known but the matrix B_p is unknown, which corresponds to the failures of power amplifiers. In the following, the reduced-order adaptive law is developed by the SPR-Lyapunov approach. Let

$$X_p = \begin{bmatrix} X^T & \dot{X}^T \end{bmatrix}^T = \begin{bmatrix} X_1^T & X_2^T \end{bmatrix}^T \tag{4.19}$$

By neglecting the disturbances, then (4.11) becomes

$$\dot{X}_1 = X_2 \tag{4.20}$$

$$\dot{X}_2 = A_{p21} X_1 + A_{p22} X_2 + B_{p2} V_c \tag{4.21}$$

Assume that all states are measurable and A_m is a stable constant matrix. By adding and subtracting $A_m X_2$ on (4.21) and using Laplace transform, we obtain

$$Z = X_2 - (sI - A_m)^{-1}[A_{p21} X_1 + (A_{p22} - A_m) X_2] = (sI - A_m)^{-1} B_{p2} V_c \tag{4.22}$$

Note that the matrix B_{p2} is the only unknown term in (4.22). By the series-parallel (SP) model, we generate

$$\hat{Z} = (sI - A_m)^{-1}\hat{B}_{p2}V_c \tag{4.23}$$

where $\hat{Z}$ and $\hat{B}_{p2}$ are the estimates of Z and B_{p2}, respectively. Then define the following auxiliary signals

$$e = Z - \hat{Z} \tag{4.24}$$

$$\tilde{B}_{p2} = \hat{B}_{p2} - B_{p2} \tag{4.25}$$

From (4.22) to (4.25), the error equation becomes

$$\dot{e} = A_m e - \tilde{B}_{p2}V_c \tag{4.26}$$

The error equation is only for analysis, not for implementation since the matrix $\tilde{B}_{p2}$ is not known exactly. Choose the Lyapunov function

$$V(e, \tilde{B}_{p2}) = e^T P_m e + tr(\tilde{B}_{p2}{}^T \Gamma^{-1} \tilde{B}_{p2}) \tag{4.27}$$

where Γ and P_m are symmetric, positive definite, constant matrices. In addition, P_m satisfies the Lyapunov equation

$$A_m{}^T P_m + P_m A_m = -Q_m \tag{4.28}$$

for some $Q_m{}^T = Q_m > 0$. Choose the adaptive law

$$\dot{\tilde{B}}_{p2} = \dot{\hat{B}}_{p2} = \Gamma P_m e V_c{}^T \tag{4.29}$$

Then the derivative of the Lyapunov function becomes

$$\dot{V} = -e^T Q_m e \le -\lambda_{\min}(Q_m)\|e\|^2 \le 0 \tag{4.30}$$

where $\lambda_{\min}(Q_m)$ is the smallest eigenvalue of Q_m.

The Lyapunov function V is positive definite and decrescent; the derivative of V is semi-definite. From the Lyapunov stability theorem, the equilibrium state $\left(e = 0, \tilde{B}_{p1} = 0\right)$ of (4.26) and (4.29) is locally uniformly stable. Assume that X_p and V_c are bounded. Then the adaptive law guarantees that $e(t) \to 0$ and $\dot{\hat{B}}_{p2} \to 0$ as $t \to \infty$, but it does not imply parameter convergence. If the plant input signals are persistently exciting, then the parameters will converge to the true values.

The second step of APPC is the controller design, which maps the estimated plant parameters to the controller parameters. The controller design in gain scheduling can be utilized. Thus, the estimated gains become

$$\hat{K}_{fb1} = \hat{B}_{p2}^{-1}(A_{p21} - A_{t21}) \tag{4.31}$$

$$\hat{K}_{fb2} = \hat{B}_{p2}^{-1}(A_{p22} - A_{t22}) \tag{4.32}$$

4.4 Simulations by Adaptive Control

An example flywheel module illustrates the operation of active FTC. Each magnetic bearing has 6 radial poles. The position stiffness matrix of two magnetic bearings is given as

$$K_{pmb} = diag\left(1.0043 \quad 1.0043 \quad 1.3754 \quad 1.3889 \quad 1.3889\right) \times 10^6 \text{ N/m}$$

Notice that the values are not influenced by the failure of power amplifiers. The control voltage stiffness matrix for no PA failed state is given as

$$K_{vmb}{}^{0} = diag\begin{pmatrix}13.1316 & 13.1317 & 13.1317 & 14.4822 & 14.4822\end{pmatrix} \text{ N/V}$$

Consider the case that two magnetic bearings have the same failure combinations and power amplifiers 1 to 3 fail consecutively. The control voltage stiffness matrices for failed states are given as follows

$$K_{vmb}{}^{1} = \begin{bmatrix} 9.8487 & -1.8954 & 0 & 0 & 0 \\ -1.8954 & 12.0374 & 0 & 0 & 0 \\ 0 & 0 & 13.1317 & 0 & 0 \\ 0 & 0 & 0 & 10.8617 & -2.0903 \\ 0 & 0 & 0 & -2.0903 & 13.2753 \end{bmatrix} \text{ N/V}$$

$$K_{vmb}{}^{12} = \begin{bmatrix} 9.8487 & -1.8954 & 0 & 0 & 0 \\ -1.8954 & 7.6601 & 0 & 0 & 0 \\ 0 & 0 & 13.1317 & 0 & 0 \\ 0 & 0 & 0 & 10.8617 & -2.0903 \\ 0 & 0 & 0 & -2.0903 & 8.4479 \end{bmatrix} \text{ N/V}$$

$$K_{vmb}{}^{123} = diag\begin{pmatrix}6.5658 & 6.5658 & 13.1317 & 7.2411 & 7.2411\end{pmatrix} \text{ N/V}$$

According to (4.13), the matrices B_{p2} corresponding to different K_{vmb} become

$$B_{p2}{}^{0} = \begin{bmatrix} 0.9315 & 0 & 0 & -0.0030 & 0 \\ 0 & 1.9737 & 0.3419 & 0 & 0 \\ 0 & 0.0030 & 0.9315 & 0 & 0 \\ -0.3419 & 0 & 0 & 1.9737 & 0 \\ 0 & 0 & 0 & 0 & 0.4430 \end{bmatrix}$$

$$B_{p2}{}^{1} = \begin{bmatrix} 0.6986 & -0.0004 & -0.1345 & -0.0023 & 0 \\ -0.0494 & 1.8092 & 0.3134 & 0.2849 & 0 \\ -0.1345 & 0.0028 & 0.8539 & 0.0004 & 0 \\ -0.2564 & 0.2849 & 0.0493 & 1.4802 & 0 \\ 0 & 0 & 0 & 0 & 0.4430 \end{bmatrix}$$

$$B_{p2}{}^{12} = \begin{bmatrix} 0.6986 & -0.0004 & -0.1345 & -0.0023 & 0 \\ -0.0493 & 1.1513 & 0.1994 & 0.2849 & 0 \\ -0.1345 & 0.0018 & 0.5434 & 0.0004 & 0 \\ -0.2564 & 0.2849 & 0.0493 & 1.4802 & 0 \\ 0 & 0 & 0 & 0 & 0.4430 \end{bmatrix}$$

$$B_{p2}{}^{123} = \begin{bmatrix} 0.4658 & 0 & 0 & -0.0015 & 0 \\ 0 & 0.9868 & 0.1710 & 0 & 0 \\ 0 & 0.0015 & 0.4658 & 0 & 0 \\ -0.1710 & 0 & 0 & 0.9868 & 0 \\ 0 & 0 & 0 & 0 & 0.4430 \end{bmatrix}$$

The disturbances are given by

$$\hat{F}_d = m_r e \omega^2 \left[\cos(\omega t) \quad \sin(\omega t) \quad \cos(\omega t + \psi) \quad \sin(\omega t + \psi) \right]^T$$

The desired closed loop matrices are given as

$$A_{t21} = 10^5 \cdot \begin{bmatrix} -1.3931 & -0.0071 & 0 & -0.0078 & 0 \\ 0 & -2.9614 & 0.8865 & -4.6622 & 0 \\ 0 & 0.0078 & -1.3931 & -0.0071 & 0 \\ -0.8864 & 4.6622 & 0 & -2.9614 & 0 \\ 0 & 0 & 0 & 0 & -2.1520 \end{bmatrix}$$

$$A_{t22} = 10^3 \cdot \begin{bmatrix} -0.1100 & 0.0004 & 0 & 0.0004 & 0 \\ 0 & -0.2331 & -0.0404 & -2.4324 & 0 \\ 0 & -0.0004 & -0.1100 & 0.0004 & 0 \\ 0.0404 & 2.4324 & 0 & -0.2331 & 0 \\ 0 & 0 & 0 & 0 & -0.5232 \end{bmatrix}$$

Then the eigenvalues of the closed loop system become

$$Eig = \begin{bmatrix} -47.810 + i2545.3 \\ -47.810 - i2545.3 \\ -185.47 + i112.64 \\ -185.47 - i112.64 \\ -54.918 + i369.3 \\ -54.918 - i369.3 \\ -54.931 + i369.07 \\ -54.931 - i369.07 \\ -261.60 + i383.1 \\ -261.60 - i383.1 \end{bmatrix}$$

4.4.1 Simulations by Gain Scheduling

When the power amplifier failures happen, a period of time (delay time) is needed to isolate the fault and to swap the feedback gains from the look-up tables. Assume that the initial failures of the power amplifiers are at 1 s, 2 s, and 3 s consecutively and the delay time is 100 ms. The control law is combined with the integrators. The rotor displacements and control magnetic forces by the gain scheduling approach are shown in Figs. 4.4 and 4.5. The rotor is continuously suspended without contacts through the entire simulation. The axial displacement due to the gravity becomes zero by using the integrator. During each delay time, the magnetic forces are reduced since the smaller matrix norms of the control voltage stiffness matrices for the failed states. The gain values for the failed states can make the closed loop responses invariant.

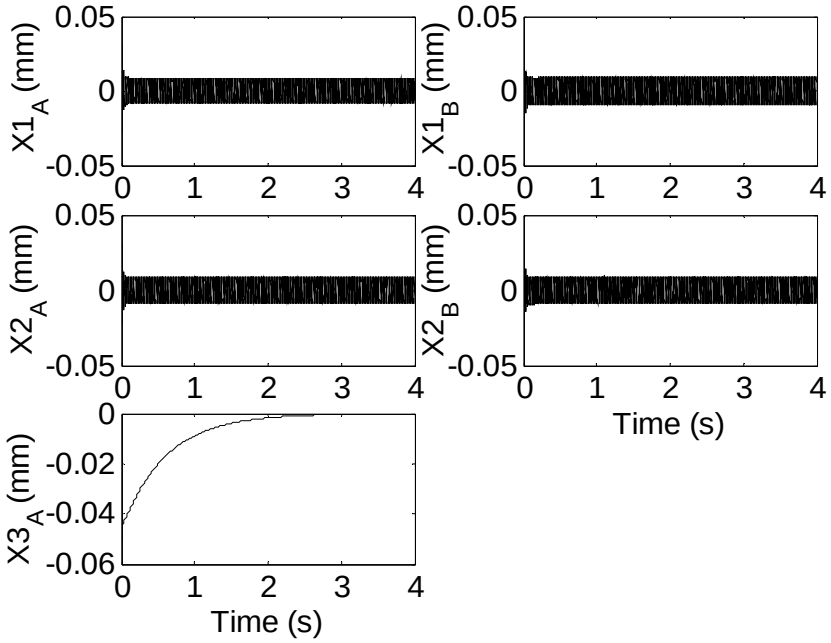

Fig. 4.4 Rotor Displacements by Gain Scheduling.

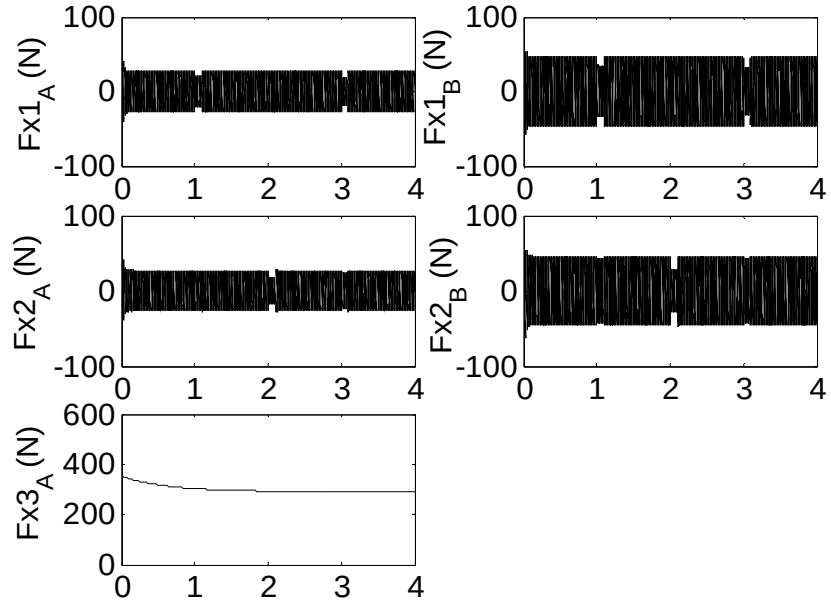

Fig. 4.5 Control Magnetic Forces by Gain Scheduling.

4.4.2 Simulations by APPC

To identify the system on-line, the inputs and outputs of the plant cannot be zero. The following reference signals and design parameter are utilized for the simulations

$$r = 2 \cdot \begin{bmatrix} \sin(20t) + \sin(25t) \\ \sin(30t) + \sin(35t) \\ \sin(40t) + \sin(45t) \\ \sin(50t) + \sin(55t) \\ \sin(60t) + \sin(65t) \end{bmatrix}$$

$A_m = -10 \cdot I_{5\times5}$, $Q_m = 100 \cdot I_{5\times5}$, and $\Gamma = 100 \cdot I_{5\times5}$.

Three examples are utilized to demonstrate the fault tolerant operation by APPC. The first example considers the case without disturbances (gravity and mass unbalance). Only consider the failures (open circuit) of the power amplifiers, and assume that the initial failures are at 20 s, 40 s, and 60 s, respectively. The rotor displacements and control magnetic forces are shown in Figs. 4.6 and 4.7, and the estimated parameters are shown in Figs. 4.8-4.12. The displacements and control magnetic forces are due to the reference signals which are necessary to identify the system parameters. The simulations show that the estimated parameters converge to the true values of each failed state by persistently exciting signals.

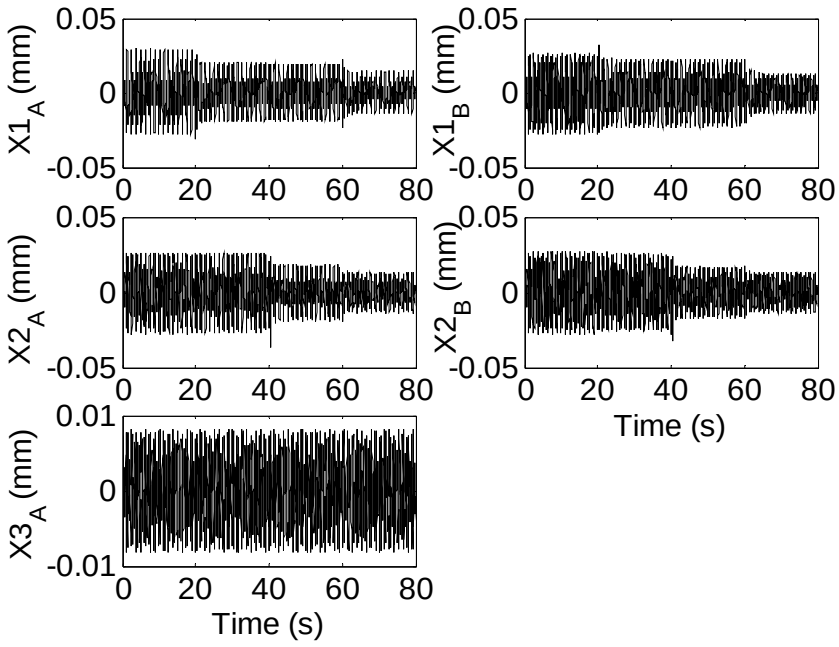

Fig. 4.6 Rotor Displacements Example 1 by APPC.

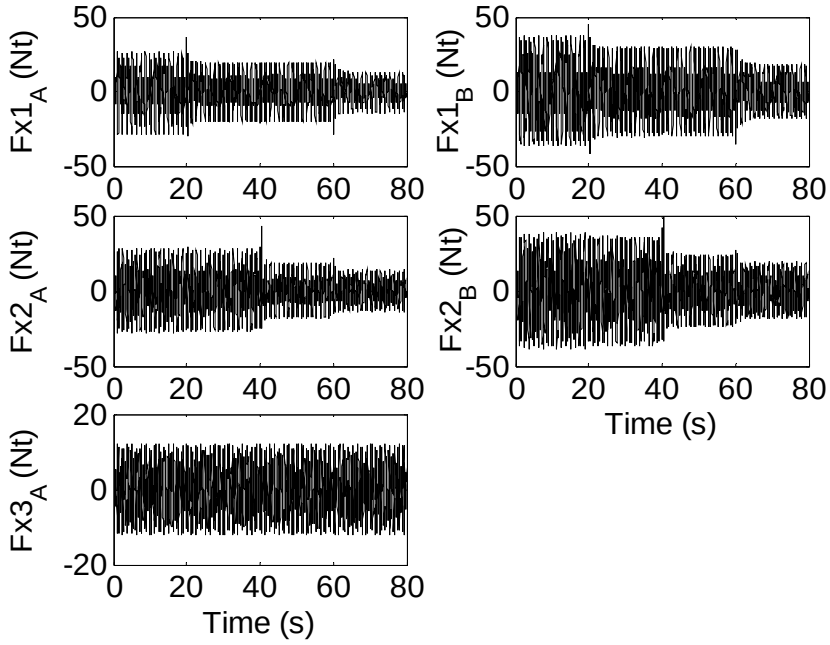

Fig. 4.7 Control Magnetic Forces Example 1 by APPC.

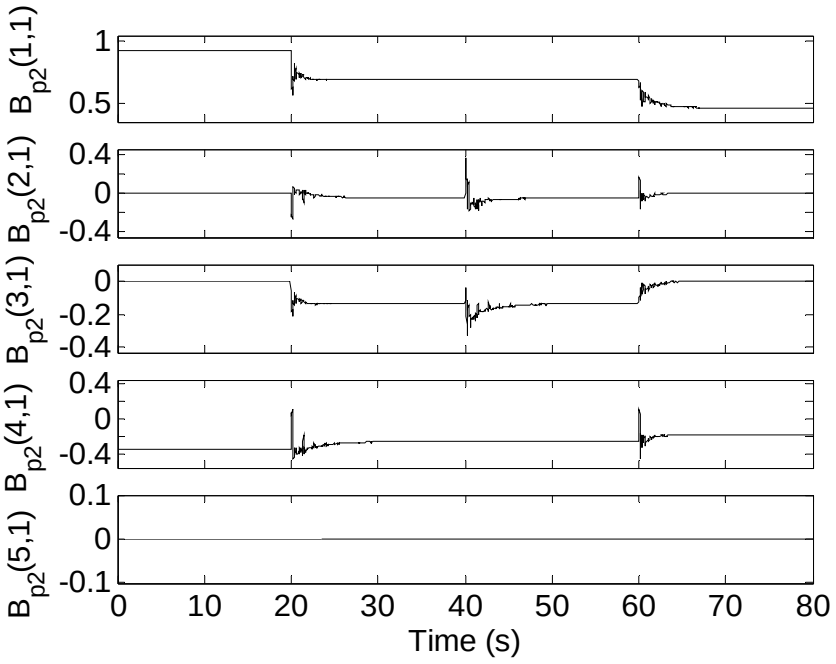

Fig. 4.8 Estimated Parameters (Column 1) Example 1 by APPC.

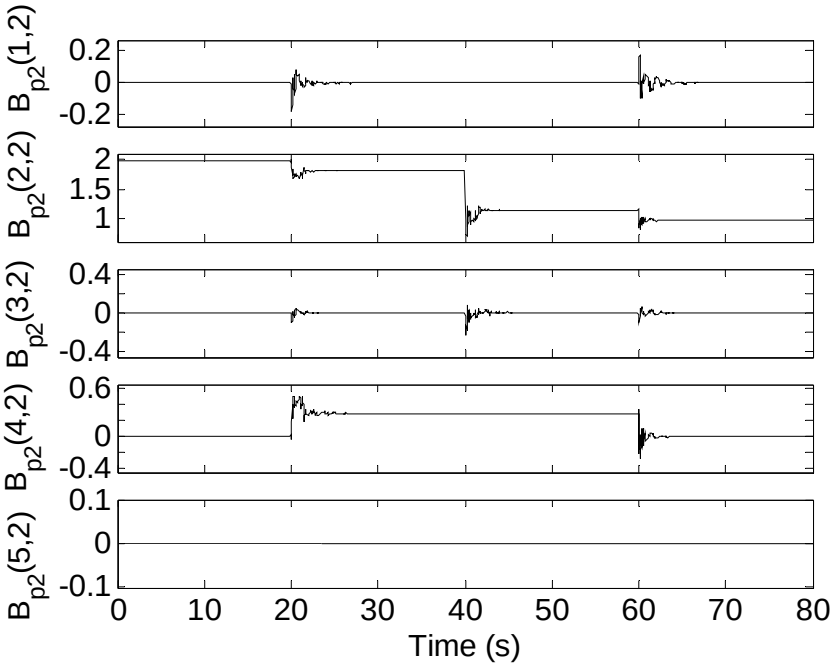

Fig. 4.9 Estimated Parameters (Column 2) Example 1 by APPC.

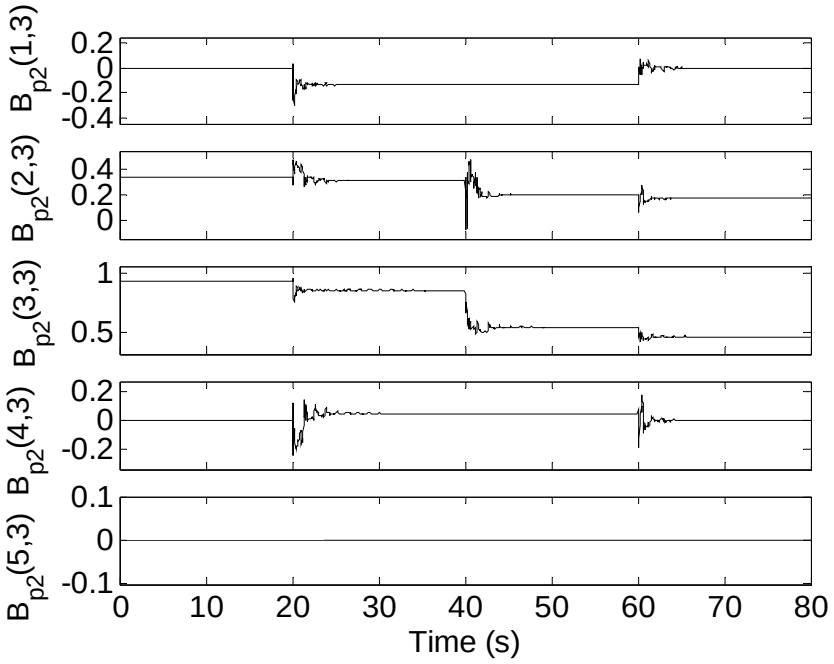

Fig. 4.10 Estimated Parameters (Column 3) Example 1 by APPC.

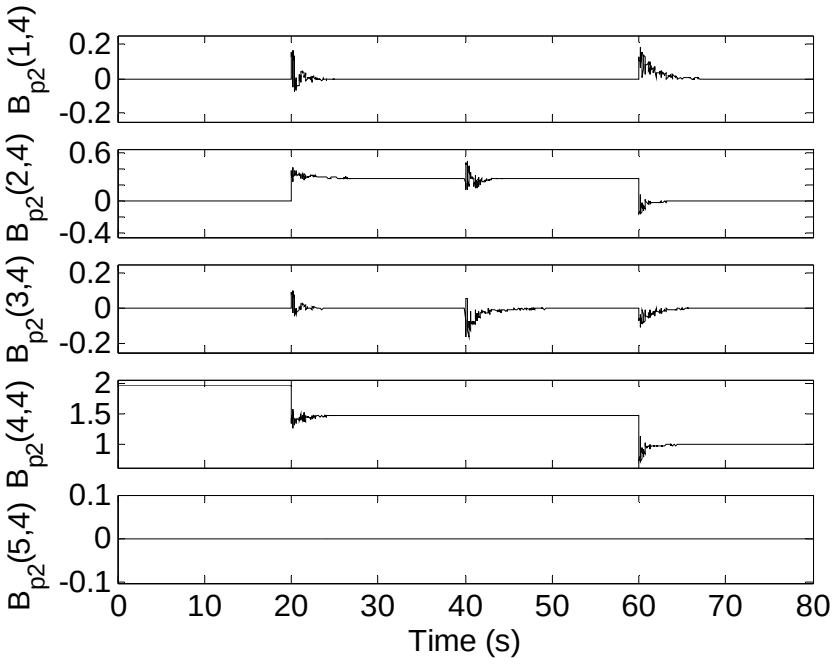

Fig. 4.11 Estimated Parameters (Column 4) Example 1 by APPC.

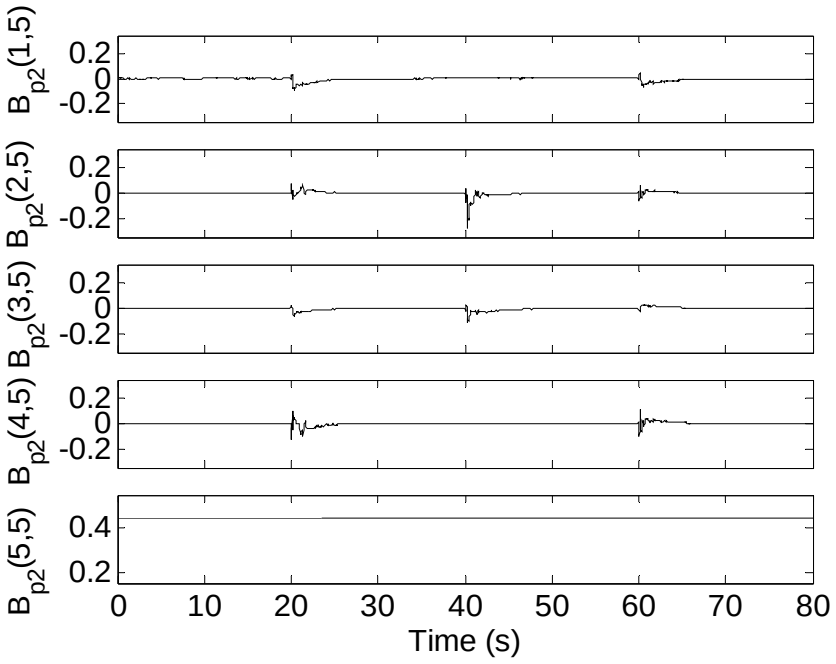

Fig. 4.12 Estimated Parameters (Column 5) Example 1 by APPC.

The values of CDMs include the power amplifier gains which may decrease over the time. In the above simulations, the power amplifier gains are fixed and have the values of 1 A/V. One advantage by APPC over the gain scheduling control is that the power amplifier gains may decrease over the time and may not be measured. Example 2 considers the case that power amplifiers fail consecutively and the power amplifier gains linearly decrease to 0.6 A/V during the entire simulation. All of the design parameters are the same as in Example 1. The rotor displacements and control magnetic forces are shown in Figs. 4.13 and 4.14. When compared with Example 1, the displacements decrease over the time. The estimated parameters are shown in Figs. 4.15-4.19. The estimated parameters follow the variations (jump and linear decreasing).

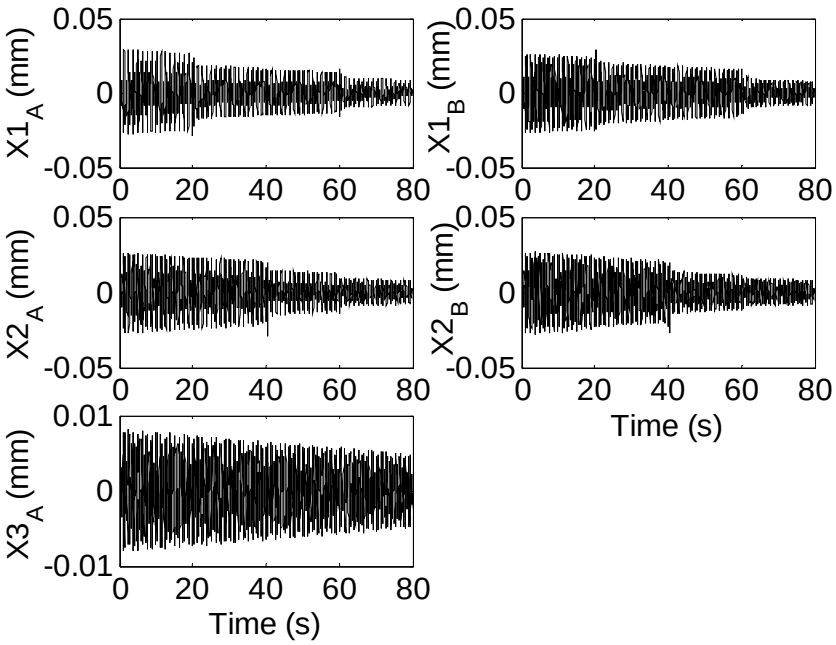

Fig. 4.13 Rotor Displacements Example 2 by APPC.

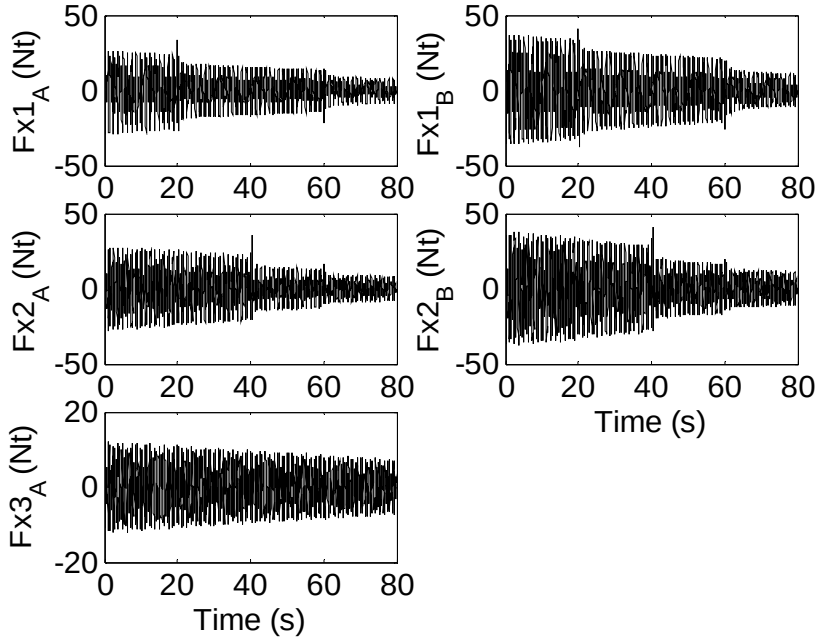

Fig. 4.14 Control Magnetic Forces Example 2 by APPC.

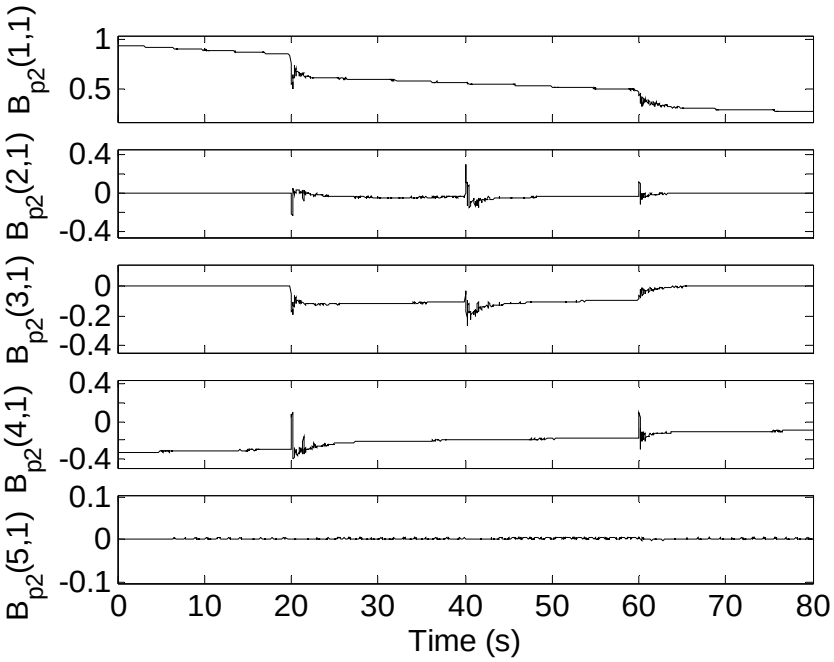

Fig. 4.15 Estimated Parameters (Column 1) Example 2 by APPC.

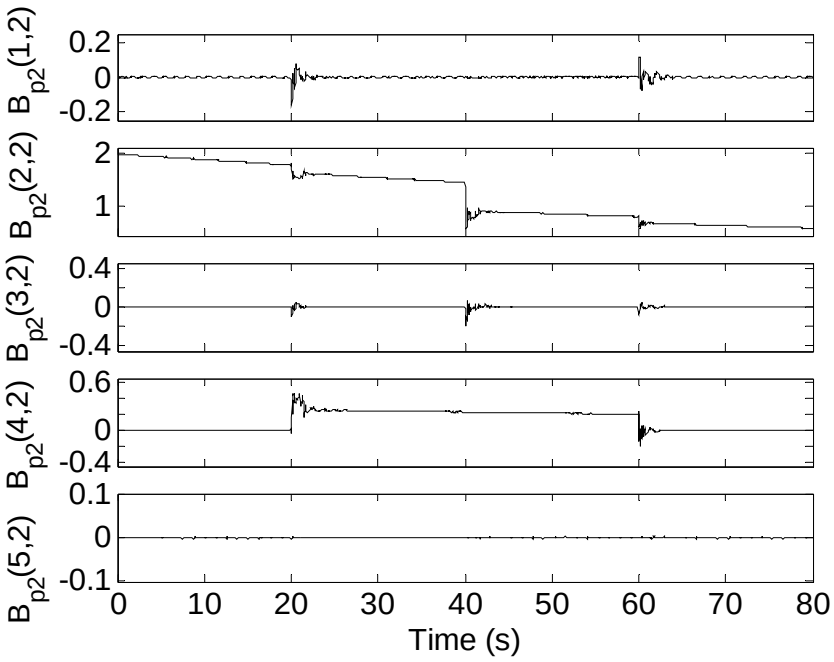

Fig. 4.16 Estimated Parameters (Column 2) Example 2 by APPC.

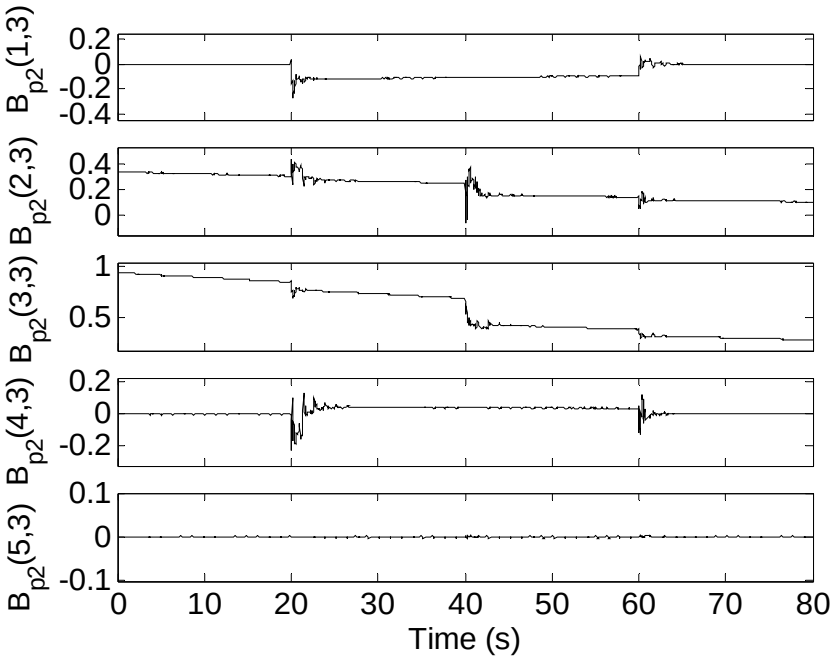

Fig. 4.17 Estimated Parameters (Column 3) Example 2 by APPC.

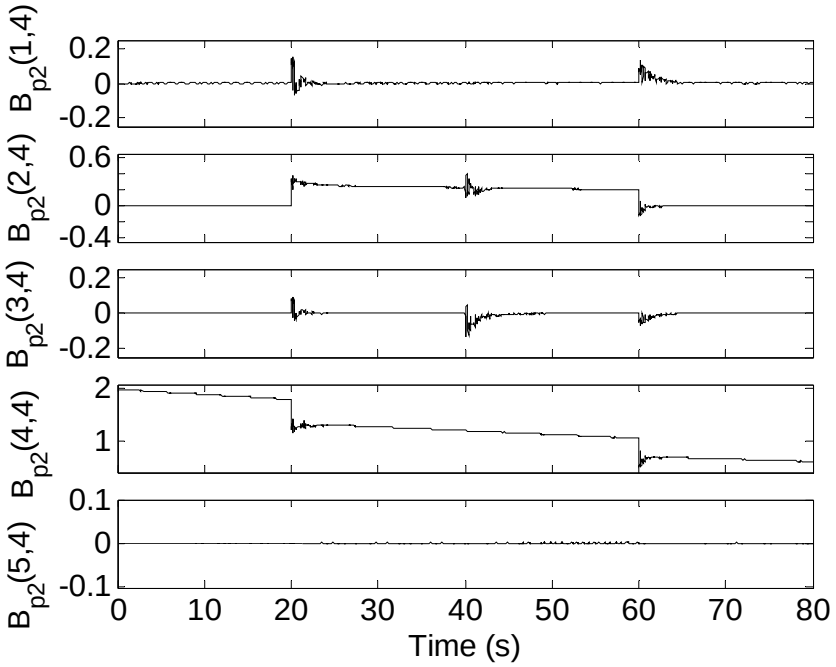

Fig. 4.18 Estimated Parameters (Column 4) Example 2 by APPC.

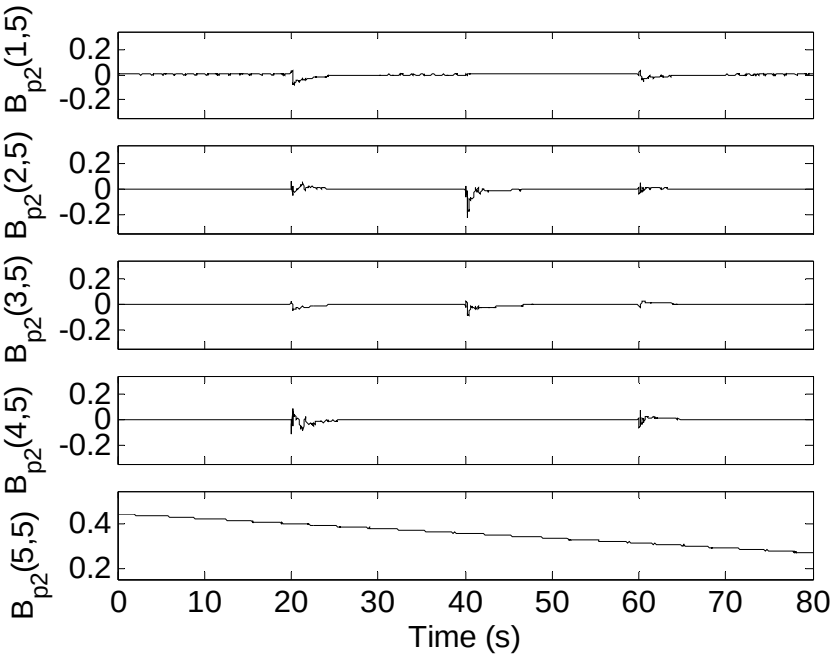

Fig. 4.19 Estimated Parameters (Column 5) Example 2 by APPC.

Example 3 considers the case with disturbances (mass unbalance and gravity). Only power amplifier failures are considered. According to [32], some filters are utilized to remove the low-frequency and known sinusoidal disturbances before the plant inputs and outputs are sent to the estimator. In the following simulations, the high pass and notch filters are utilized to remove the gravity in the axial direction and the mass unbalances in the radial directions, respectively. The following design parameters are utilized for the simulations. $A_m = -10 \cdot I_{5\times5}$, $Q_m = 10 \cdot I_{5\times5}$, and

$$\Gamma = diag(1 \quad 1 \quad 1 \quad 1 \quad 0.1)$$

The frequencies of the reference signals are the same as before, but their amplitudes are increased to 5 (V) to help identify the parameters. In addition, assume that the initial failures of the power amplifiers are at 200 s, 400 s, and 600 s, respectively.

The displacements and control magnetic forces are shown in Figs. 20 and 21. The responses are due to the disturbances and reference signals, and their amplitudes are much large when compared with the gain scheduling approach. The estimated parameters are shown in Figs. 22-26. Due to the small adaptive gains, the parameters slowly converge to the true values or the values with steady state errors.

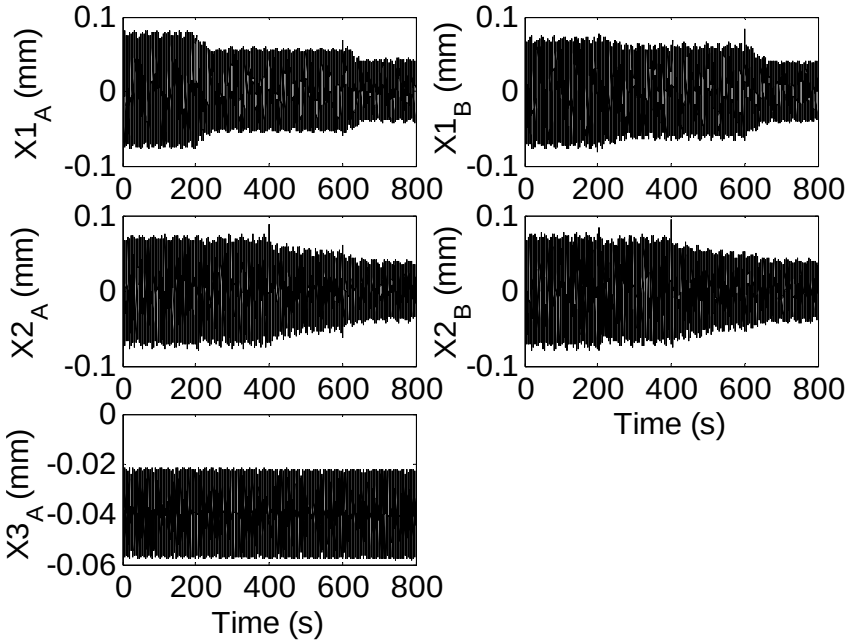

Fig. 4.20 Rotor Displacements Example 3 by APPC.

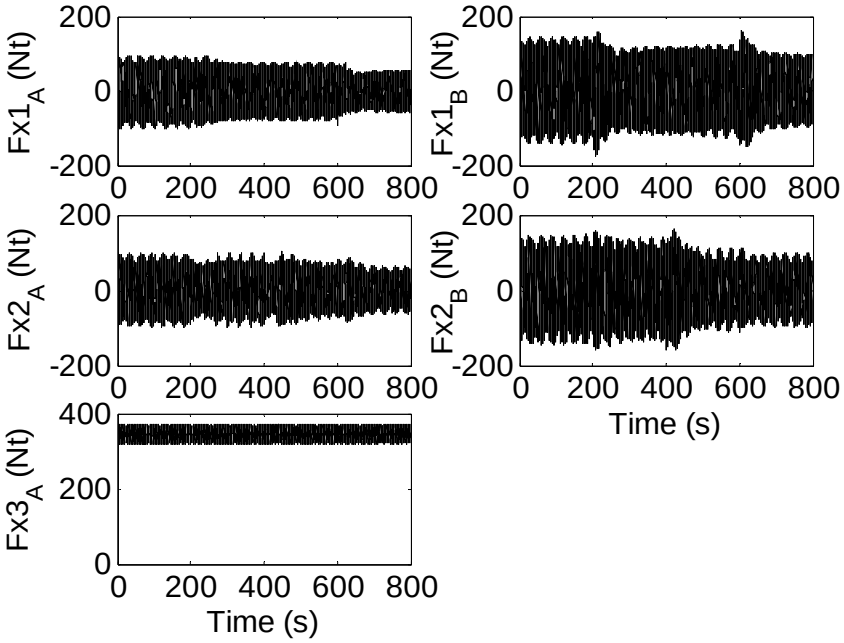

Fig. 4.21 Control Magnetic Forces Example 3 by APPC.

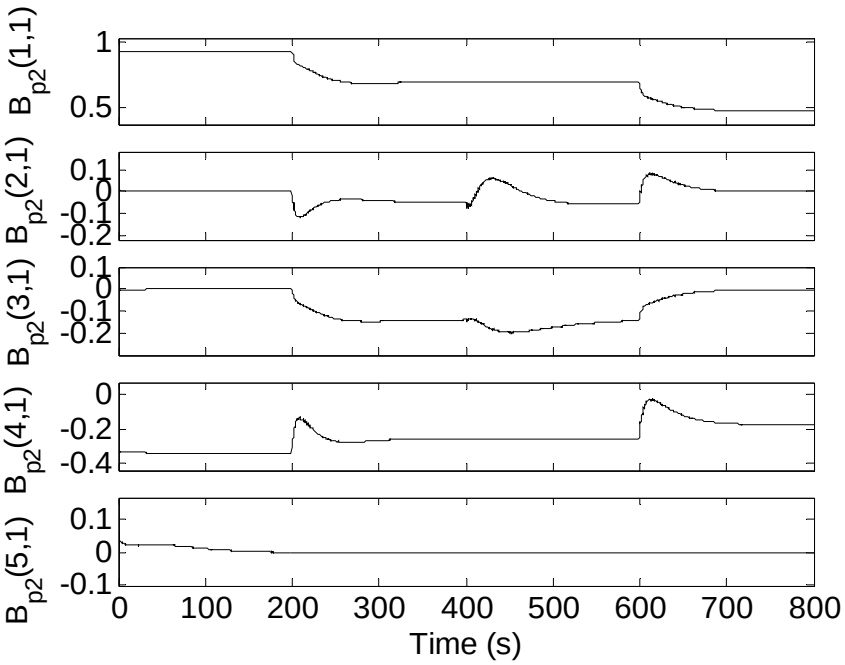

Fig. 4.22 Estimated Parameters (Column 1) Example 3 by APPC.

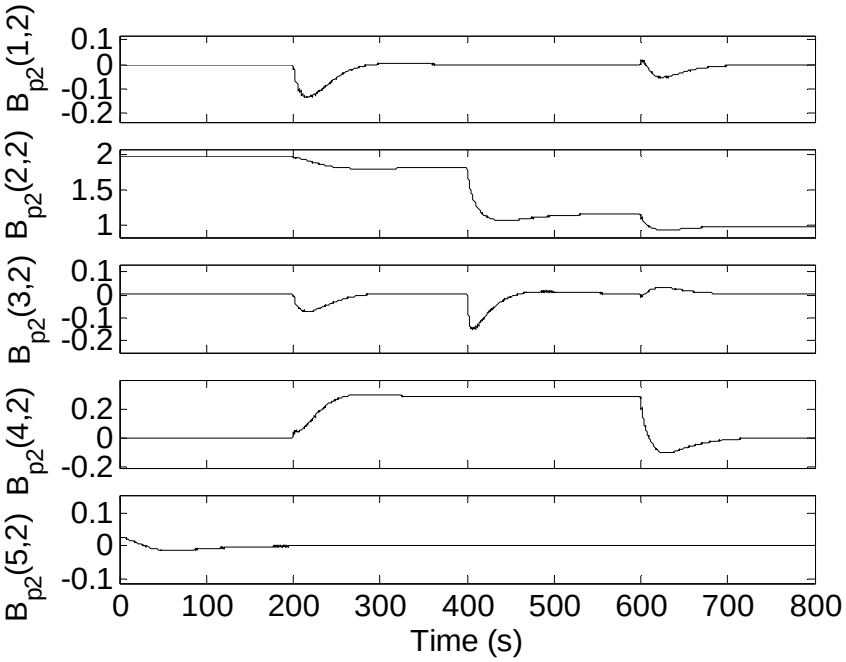

Fig. 4.23 Estimated Parameters (Column 2) Example 3 by APPC.

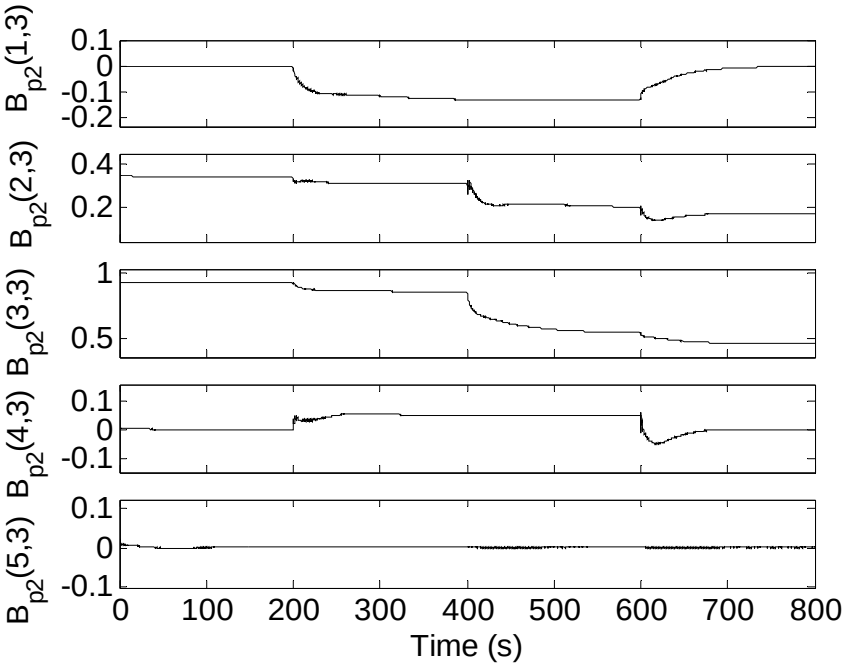

Fig. 4.24 Estimated Parameters (Column 3) Example 3 by APPC.

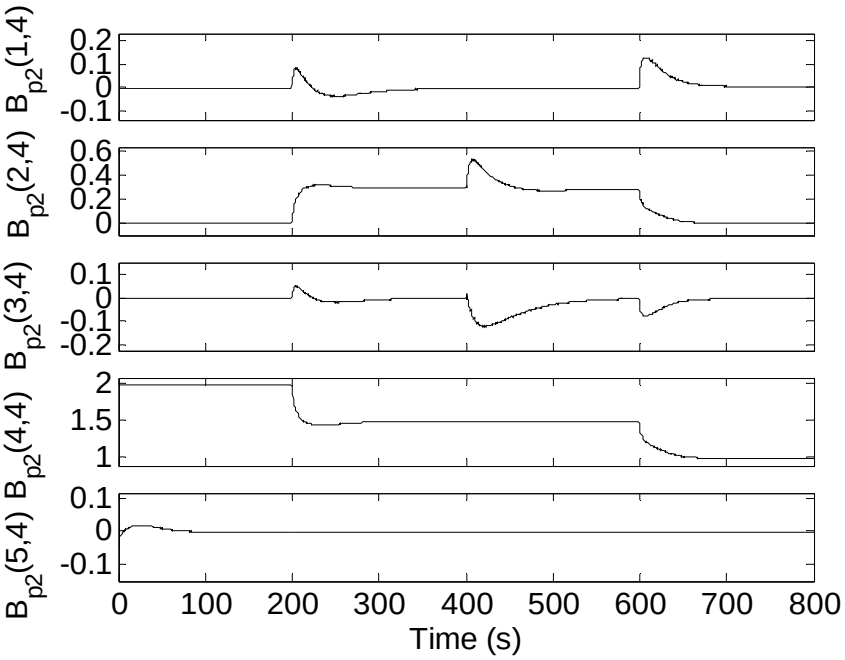

Fig. 4.25 Estimated Parameters (Column 4) Example 3 by APPC.

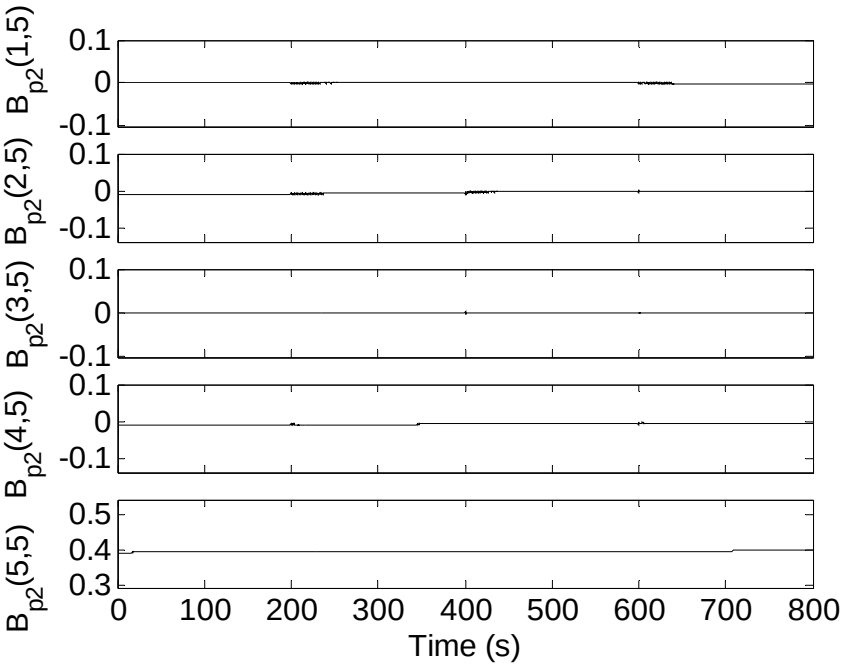

Fig. 4.26 Estimated Parameters (Column 5) Example 3 by APPC.

CHAPTER V

CONCLUSION AND FUTURE RESEARCH

5.1 Conclusion

This dissertation presents the fault tolerant control of homopolar magnetic bearings and sensor arrays. Successful fault tolerant control has been demonstrated by two approaches. One approach is to adjust system parameters by swapping current distribution matrices for magnetic bearings and weighting gain matrices for sensor arrays, but maintain the MIMO-based control law invariant before and after the faults. The other is to adjust the feedback gains on-line or off-line, but the current distribution matrices are invariant before and after the faults. Both approaches can compensate for the failures (open circuit) of power amplifiers (or coils) and sensors. The simulations show some interesting results and trends which are summarized as follows.

5.1.1 Fault Tolerant of Homopolar Magnetic Bearings

Current distribution matrices are evaluated based on the set of poles (power amplifier plus coil) that have failed and the requirements for uncoupled force/voltage control, linearity, and specified force/voltage gains to be unaffected by the failure. The first advantage of homopolar magnetic bearings over heteropolar magnetic bearings is the automatic invariance of the position stiffness before and after pole failure, and the second advantage is the high efficiency since the bias flux of HOMB is supplied by permanent magnets.

Among 4, 6, and 7 pole homopolar magnetic bearings, successful levitation with 2 unfailed radial poles is demonstrated, and the bearing reliability is increased as the number of poles increases.

5.1.2 Fault Tolerant of Circular Sensor Arrays

Weighting gain matrices are evaluated based on the set of sensors that have failed and the requirements for uncoupling x_1 and x_2 sensing, runout reduction, and voltage/displacement gains to be unaffected by the failure. The simulations and analysis presented have confirmed the ability of sensor arrays to eliminate sensor runout. It has been shown that the more sensors the array has, the more harmonics of runout the array can eliminate or reduce. Complete runout elimination can be maintained by the SIA if some sensors fail, but not by the NSIA. Judging from the reliability and runout reduction probability, SIA is better than NSIA, but of course requires additional hardware for faulted sensor detection.

Since sensor arrays use more sensors that have failure probability, the array reliability and runout reduction, which depend on one single sensor reliability, have to be considered. Two criteria are defined to evaluate the sensor array reliability and runout reduction probability. A more precise way to decide the array reliability is to do system simulations in all failure combinations. A sensor array with n sensors has (2^n-1) failure combinations. When n is large, the simulations for all failure combinations are time consuming and impractical.

It is a trade-off to decide how many sensors in an array and how many harmonics of runout are considered. If the number of runout harmonics is decided, in general the

more sensors the array has, the higher system reliability and runout reduction probability the array can reach when r_s is higher. In addition, the runout reduction performance is not guaranteed for those harmonics of runout which are not considered in the constraint equations.

5.1.3 Adaptive Fault Tolerant Control

The simulation results have demonstrated the fault tolerance of power amplifier failures by two adaptive control schemes. The gain scheduling adaptive control is robust to the disturbances (gravity and mass unbalance), but the information for failure configurations is required in advance to build up the feedback gains in the look-up table.

The adaptive law for the linear time invariant plant is utilized to accommodate the parameter jump. The persistently exciting signals are required to make the jump parameters converge to the true values of each failed state. However persistent excitation contradicts the objectives of the regulators and cannot, in general, be avoided.

The amplitudes and frequencies of the reference signals will influence the rate of parameter convergence. Generally speaking, the larger amplitudes the reference signals have, the faster the parameters can converge to the true values. Similarly, high adaptive gains (Q_m and Γ) can make the parameters converge fast as well, but may make the closed loop unstable when disturbances are considered.

5.2 Future Research

The adaptive law in Section 4.3 is not robust with respect to the bounded, unknown disturbances. In addition, the states of controller, actuators, and sensors are

neglected in Section 4.3. The adaptive law may excite the un-modeled dynamics. Future research may develop the robust adaptive pole placement control scheme, which is robust with respect to bounded, unknown disturbances and un-modeled dynamics.

In Chapter III, the non-swapping-in WGMs approach also makes the voltage/displacement gains jump. Future research may utilize the adaptive control scheme to accommodate the sensor failures.

REFERENCES

[1] Iwaki, S., 1990, “The Optimal Location of Electromagnets in Multiple Degree of Freedom Magnetically Suspended Actuators,” ASME J. Dynamic Systems, Measurement, and Control, **112**(4), pp. 690-695.

[2] Meeker, D. C., 1996, “Optimal Solution to the Inverse Problem in Quadratic Magnetic Actuators,” Ph.D. dissertation, Univ. of Virginia, Charlottesville, VA.

[3] Maslen, E. H., and Meeker, D. C., 1995, “Fault Tolerance of Magnetic Bearings by Generalized Bias Current Linearization,” IEEE Trans. Magnetics., **31**(3), pp. 2304-2314.

[4] Maslen, E. H., Sortore, C. K., and Gillies, G. T., 1999, “Fault Tolerant Magnetic Bearings,” ASME J. Engineering for Gas Turbines and Power, **121**(3), pp. 504-508.

[5] Na, UJ, and Palazzolo, A., 2000, “Optimized Realization of Fault-Tolerant Heteropolar Magnetic Bearings,” ASME J. Vibration and Acoustics, **122**(3), pp. 209-221.

[6] Na, UJ, Palazzolo, A., and Provenza, A., 2002, “Test and Theory Correlation Study for a Flexible Rotor on Fault-Tolerant Magnetic Bearings,” ASME J. Vibration and Acoustics, **124**(3), pp. 359-366.

[7] Na, UJ, and Palazzolo, A., 2000, “Fault Tolerance of Magnetic Bearings with Material Path Reluctances and Fringing Factors,” IEEE Trans. Magnetics, **36**(6), pp. 3939-3946.

[8] Maslen, E. H., Allaire, P. E., Noh, M. D., and Sortore, C. K., 1996, “Magnetic Bearing Design for Reduced Power Consumption,” ASME J. Tribology, **118**(4), pp. 839-846.

[9] Batty, R., 1988, “Notch Filter Control of Magnetic Bearings to Improve Rotor Synchronous Response,” MS thesis, Massachusetts Institute of Technology, Cambridge, MA.

[10] Knospe, C. R., 1991, “Stability and Performance of Notch Filters for Unbalance Response,” *Proceedings of the International Symposium on Magnetic Suspension Technology*, Hampton, VA., p. 181.

[11] Bleuler, H., Gahler, C., Herzog, R., Larsonneur, R., Mizuno, T., Siewart, R., and Woo, S.-J, 1994, "Application of Digital Signal Processors for Industrial Magnetic Bearings," IEEE Trans. on Control Systems Technology, **2**(4), pp. 280-289.

[12] Herzog, R., Buhler, P., Gahler, C., and Larsonneur, R., 1996, "Unbalance Compensation Using Generalized Notch Filters in Multivariable Feedback of Magnetic Bearings," IEEE Trans. on Control Systems Technology, **4**(5), pp. 580-586.

[13] Na, H.–S., and Park, Y., 1997, "An adaptive Feedforward Controller for Rejection of Periodic Disturbances," J. Sound and Vibration, **201**(4), pp. 427-435.

[14] Knospe, C. R., Tamer S. M., and Fedigan, S. J., 1997, "Synthesis of Robust Gain Matrices for Adaptive Rotor Vibration Control," ASME J. Dynamic Systems Measurement, and Control, **119**(2), pp. 298-300.

[15] Knospe, C. R., and Tamer S. M., 1997, "Experiments in Robust Control of Rotor Unbalance Response Using Magnetic Bearings," Mechatronics, **7**(3), pp. 217-229.

[16] Knospe, C. R., Tamer S. M., and Fedigan, S. J., 1997, "Robustness of Adaptive Rotor Vibration Control to Structured Uncertainty," ASME J. Dynamic Systems Measurement, and Control, **119**(2), pp. 243-250.

[17] Betschon, F., and Knospe, C. R., 2001, "Reducing Magnetic Bearing Currents via Gain Scheduled Adaptive Control," IEEE/ASME Trans. on Mechatronics, **6**(4), pp.437-443.

[18] Kim, C.-S., and Lee, C.-W., 1997, "In Situ Runout Identification in Active Magnetic Bearing System by Extended Influence Coefficient Method," IEEE/ASME Trans. on Mechatronics, **2**(1), pp. 51-57.

[19] Setiawan, J. D., Mukherjee, R., and Maslen, E. H., 2001, "Adaptive Compensation of Sensor Runout for Magnetic Bearings with Uncertain Parameters: Theory and Experiments," ASME J. Dynamic Systems, Measurement, and Control, **123**(2), pp. 211-218.

[20] Setiawan, J. D., Mukherjee, R., and Maslen, E. H., 2002, "Synchronous Sensor Runout and Unbalance Compensation in Active Magnetic Bearings Using Bias

Current Excitation," ASME J. Dynamic Systems, Measurement, and Control, **124**(1), pp. 211-218.

[21] Tao, G., Joshi, S. M., and Ma, X., 2001, "Adaptive State Feedback and Tracking Control of Systems with Actuator Failures," IEEE Trans. on Automatic Control, **46**(1), pp. 78-95.

[22] Tao, G., Chen, S., and Joshi, S. M., 2002, "An Adaptive Actuator Failure Compensation Controller Using Output Feedback," IEEE Trans. on Automatic Control, **47**(3), pp. 506-511.

[23] Tao, G., Chen, S., and Joshi, S. M., 2002, "An Adaptive Control Scheme for Systems with unknown Actuator Failures," Automatica, **38**(6), pp. 1027-1034.

[24] Skogestad, S. and Postlethwaite, I., 1996, *Multivariable Feedback Control*, John Wiley & Sons, New York, p. 519, Appendix A.

[25] Sun, G., Palazzolo, A., and Kaushik, N., 2003, "An Efficient Algorithm for Blade Loss Simulations Using a High Fidelity Ball Bearing and Damper Model," *ASME Design Engineering Technical Conferences and Computers and Information in Engineering Conference*, Chicago, IL, pp. 1011-1020.

[26] Okada, Y., Nagai, B. and Shimane, T., 1992, "Cross Feedback Stabilization of the Digitally Controlled Magnetic Bearing," ASME J. Vibration and Acoustics, **114**(1), pp. 54-59.

[27] Ahrens, M., Traxler, A., Von Burg, P., and Schweitzer, G., 1994, "Design of a Magnetically Suspended Flywheel Energy Storage Device," *Fourth International Symposium on Magnetic Bearings*, ETH Zurich, Switzerland, pp. 553-558.

[28] Ahrens, M., Kucera, L., and Larsonneur, R., 1996, "Performance of a Magnetically Suspended Flywheel Energy Storage Device," IEEE Trans. on Control System Technology, **4**(5), pp. 494-502.

[29] Kuo, W., and Zuo, M., 2003, *Optimal Reliability Modeling*, John Wiley & Sons, Hoboken, p. 231, Chap. 7.

[30] Ben-Israel, A., and Greville, T., 2003, *Generalized Inverses: Theory and Applications*, Springer-Verlag, New York, p. 105.

[31] Ioannou, P. A., and Sun, J., 1995, *Robust Adaptive Control*, Prentice Hall PTR, River, NJ, pp. 325-327.

[32] Astrom, K. J., and Wittenmark, B., 1995, *Adaptive Control*, Addison-Wesley, New York, pp. 494-495.

VITA

Ming-Hsiu Li was born on September 16, 1970, in Taichung County, Taiwan. He is the first child among four in the family of Shan-Tsao Li. He received his Bachelor of Science degree in agricultural machinery engineering from National Chung Hsing University, Taiwan, in June of 1994 and Master of Science degree in aeronautics and astronautics engineering from National Cheng Kung University, Taiwan, in June of 1996. After a two-year military service in the army and one-and-a-half years as a mechanical engineer in Phoenixtec Power Co., he enrolled in the Ph.D. program in mechanical engineering of Texas A&M University in August of 2000. After passing the qualifying exam and finishing some course work, he has worked with Dr. Palazzolo in the Vibration Control and Electromechanics Lab (VCEL) since April of 2002. Most of his research is focused on the fault tolerant control of magnetic bearings.

Ming-Hsiu may be reached at the following address:

6, Ln. 428, Chung-Cheng N. Rd,

Sanchung, Taipei County, 241

Taiwan